RSC Advances

PAPER

View Article Online
View Journal | View Issue

Cite this: *RSC Adv.*, 2020, **10**, 21914

A new dendrimer series: synthesis, free radical scavenging and protein binding studies†

Dhaval Makawana and Man Singh *

Tri-*o*-tolyl benzene-1,3,5-tricarboxylate (TOBT (**T0**)), tri-4-hydroxyphenyl benzene-1,3,5-tricarboxylate (THBT (**T1**)), and tri-3,5-dihydroxyphenyl benzene-1,3,5-tricarboxylate (TDBT (**T2**)), a series of 1st tier dendrimers with a common 1,3,5-benzenetricarbonyl trichloride/trimesoyl chloride (TMC) core, are reported. **T0** does not have any replaceable H^+ on its terminal phenyl group, acting as a branch. **T1** has one phenolic –OH at the *para* position and **T2** has two phenolic –OH groups at the 3 and 5 positions of each terminal phenyl group. During synthesis, these –OH groups at the terminal phenyl groups were protected through *tert*-butyldimethylsilyl chloride (TBDMSCl) assisted with *t*-BuOK in DCM, THF, indazole, 4-dimethylaminopyridine (DMAP), and tertiary-*n*-butyl ammonium fluoride (TBAF). MTBDMSP (mono-tertiary butyl dimethylsilane phloroglucinol), DTBDMSP (di-tertiary butyl dimethylsilane phloroglucinol), and TTBDMSP (tri-tertiary butyl dimethylsilane phloroglucinol) were obtained with >90% yield, and TTBDMSP phenolic derivatives (PDs) were developed to synthesize **T0**, **T1**, and **T2** dendrimers by deprotecting with TBAF. **T0** showed superhydrophobic properties as it did not dissolve in methanol, contrary to **T1** and **T2**, but dissolved in acetone. Their structures were determined using ^{1}H and ^{13}C NMR spectroscopies, and mass spectrometry. Their scavenging activities were studied using UV-Vis spectrophotometry compared with ascorbic acid and protein binding was studied with bovine serum albumin (BSA) and lysozyme (lyso). **T0** exhibited exceptional optical activity contrary to **T1** and **T2**, which acted as antioxidants to scavenge free radicals.

Received 7th May 2020
Accepted 25th May 2020

DOI: 10.1039/d0ra04102e

rsc.li/rsc-advances

1. Introduction

Generally, webdrimers like PAMAM (poly(amidoamine)) or starburst dendrimers with repeated branched subunits of amide and amine functionality, like TTDMM (trimesyol-1,3,5-trimethyl malonate), TSMM (trisurfactantomethylol melamine), and others do not have replaceable hydrogen atoms. Therefore, they are only capable of binding bionanoparticles, transporting them, and releasing them at desired sites as they have adequate steric activities, which are generated by their branches to encapsulate the drugs or genes safely. The branching induces the required rotational, vibrational and translational motions without altering the chemical activities of their void spaces, which is supportive of safer encapsulation. Thus, these webdrimers act as ideal gene delivery vehicles. To date, no webdrimer has been reported that can liberate H^+ ions or protons, while also behaving as a drug or gene delivery vehicle. Such dendrimers behave differently in acidic and alkaline chemical environments, so they are medium selective moieties. Also, these webdrimers liberate protons when there is spontaneity for them, otherwise they do not liberate or furnish protons. Dendrimers remain monodispersed in the desired solvents and do not strongly bind or aggregate together and they maintain higher surface area, which is a most desired characteristic for molecular sensors. Dendrimers as multifunctional nanomaterials are compatible in nature so their physicochemical properties are a thrust area of current research. Dendrimers do not have structural constituents to support electronic transitions from the HOMO to LUMO state apart from scavenging activities. Detection of the scavenging activities of free radicals (FRs) is a major challenge in the food industry, biochemical reactions, and bioengineering due to the thermodynamically and kinetically active chemical moieties.[1] FR scavenging has become an inevitable task to prevent the damage of valuable chemical processes of biomolecules and their combinations by FRs.[1–3] FRs have lone pair electrons (LPEs), π-conjugation, sigma bonds, and functional groups to intensify the FR activities. Sensors may attract FRs to void spaces to immobilize them through van der Waals forces.[4] Antioxidants are extensively used to prevent the threat of chronic diseases such as cancer and cardiovascular diseases, along with other irregular functions in cells.[5,6] For the last few decades, synthetic molecules have been used to prevent redox, but they have a lower number of phenolic –OH.[7] Flavonoids with large –OH numbers to release protons for scavenging are being synthesized. Vitamin

School of Chemical Sciences, Central University of Gujarat, Gandhinagar-382030, India. E-mail: dhavalmak@cug.ac.in; mansingh50@hotmail.com

† Electronic supplementary information (ESI) available. See DOI: 10.1039/d0ra04102e

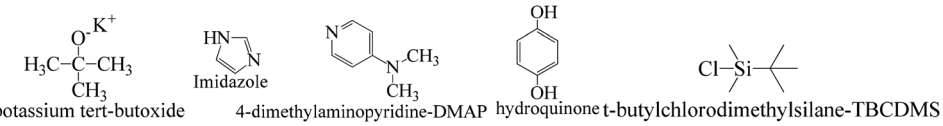

Scheme 1 Functional structures of the molecules used as catalysts and protection and deprotection agents.

C, beta-carotene, and polyphenolic flavonoids are used as a source of antioxidants in the diet. Flavonoids provide labile H^+ to sense FRs, and accommodate the pH and potential energies of biologically and biochemically active liquid mixtures against oxidative deformation of molecular structures.[1,4,8–10] The solubility of polyphenols in aqueous systems is negligible. Antioxidant effectiveness *in vitro* measures the radical scavenging activity (RSA) against FRs: singlet oxygen ($^1O_2$), superoxide radical anions ($O^{2\bullet-}$), hydroxyl radicals ($^\bullet OH$) and hydrogen peroxide.[5,7,11] **T1** and **T2** have –OH and functional void spaces with π-conjugation favorable to release H^+ in steps and scavenge FRs. No such dendrimer antioxidants have been reported yet, where phenolic molecules are used as the core as well as branches. These have higher stability with void spaces, and steric ability.[12–14] These induce rotational, translational, vibrational, oscillatory and electronic motions to encapsulate a drug.[10,14–16] Liu and co-workers have used DPPH radicals with stronger scavenging of natural antioxidants in combination than individual antioxidants.[17] More phenolic –OH groups in a molecule act as effective antioxidants due to intramolecular synergistic activities with certain tentropy among them.[18] Nishiyama and coworkers have investigated intramolecular synergistic activities between chromanol and thiopropionate groups of a series of antioxidants in tetralin oxidation.[19,20] Dendrimers with a web-like structure are a class of functional webdrimer molecules that have functional void spaces for drug or gene binding, transport and release. They do not affect the chemical environment, like pH, ionic strength, temperature or aggregation of biochemical, biological, and biophysical processes as they do not undergo dissociation, ionization, or dimerization. The webdrimers remain monodispersed with larger surface area and surface activities with comparatively higher entropy than ordinary molecules. So, they have extraordinarily stronger drug or nanoparticle binding and transporting abilities in media of wider pH, as they are least affected by the pH variations of a process. The novelty of these molecules is that they do not undergo any structural changes within the infinitesimal thermodynamic conditions as they have a unique structure, including a core and branching, which mutually stabilizes and chemically balances their chemical activities, allowing them to remain stabilized.

2. Experimental and methods

2.1 Materials for conducting the reaction

TMC procured from Sigma Aldrich was used as received; *o*-cresol, hydroquinone, phloroglucinol, and potassium *tert*-butoxide were obtained from Sisco Research Laboratories Pvt. Ltd. India. Structures were determined with ^1H NMR and ^{13}C NMR spectra recorded in $CDCl_3$ and $DMSO_4$ (NMR grade, 99.99% yield) with a Bruker Biospin Avance-III 500 MHz FT-NMR. TMS was used as an internal standard due to its highest shielding state. 99% pure solvents procured from Rankem were used. Analytical thin-layer chromatography (TLC) was performed with pre-coated silica gel plates (200 μm) with fluorescent indicator acquired from Sigma Aldrich. For flash column chromatography, silica of 200–400 mesh size procured from SRL was used. Imidazole and *t*-BuOK maintained a basic medium in protecting the phenolic groups with TBCDMS and deprotection with TBAF during synthesis, which was catalyzed by DMAP. For clarity of their participation in the chemical processes, the chemical structures are given in (Scheme 1).

2.2 Protection and deprotection of phenolic derivatives

2.2.1. Hydroquinone protection. Imidazole (2.2 mM) and DMAP (0.06 g, 0.5 mmol%) were added to hydroquinone (HQ) solution (1 eq. 10 mM) in dry DCM (50 ml) and were

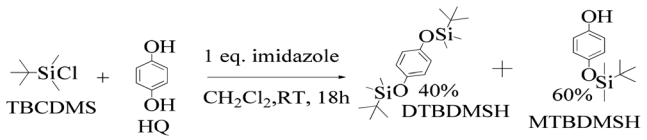

Scheme 2 The mechanism of the reaction in the prescribed medium and experimental conditions. Imidazole is a base and attracts H^+ from HQ and gains a positive charge by transferring its LPE to a H^+ ion, which attracts Cl^- from TBCDMS, and it catalyzes the reaction as shown in Scheme 3.

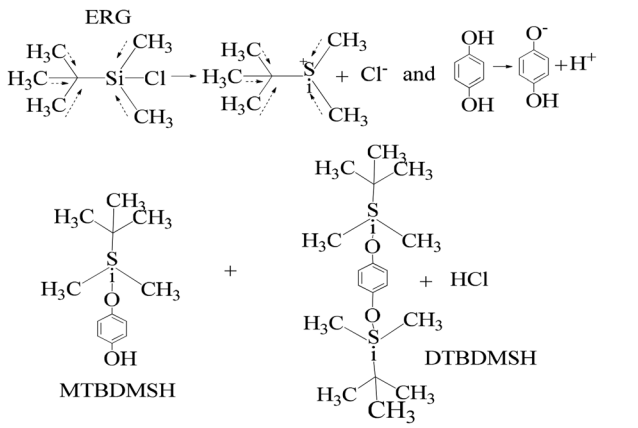

Scheme 3 The charge orientation mechanism to develop nucleophilic and electrophilic centers to conduct the reaction in the prescribed medium and experimental conditions.

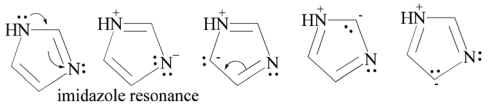

Scheme 4 The charge orientation mechanism of the imidazole structure to develop nucleophilic and electrophilic centers to conduct the reaction in the prescribed medium.

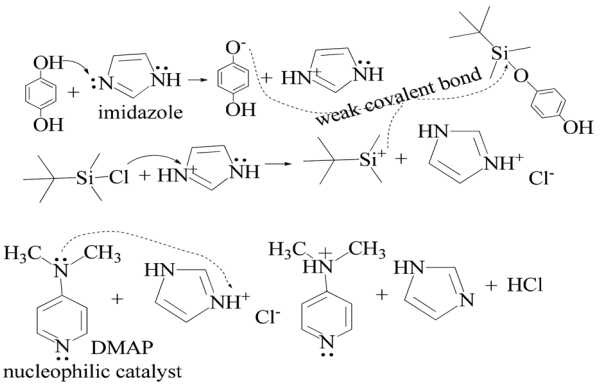

Scheme 5 The proton shift from dihydroxybenzene to imidazole to sustain a reaction in collaboration with DMAP for the protection mechanism *via* nucleophilic and electrophilic centers in the prescribed medium and experimental conditions.

homogenized. *t*-Butylchlorodimethylsilane (TBCDMS) (1.0 eq., 10 mM) solution in DCM (20 ml) was prepared separately and was added into HQ solution dropwise. The solvent remained common in the process. The reaction mixture was stirred for 24 h @ 700 rpm and the reaction was stopped by adding brine (100 ml). This developed aqueous and organic liquid phases. The aqueous phase was further treated with DCM (3×50 ml) to extract the compound if it went into the aqueous phase, which was added with organic phase. The organic phase dried over anhydrous Na_2SO_4 was concentrated under vacuum by evaporation. The residue was purified with flash chromatography using a hexane and ethyl acetate mixture in a 4 : 1 ratio, which gave a colorless solid (55%).[33] DTBDMSH (di-tertiary butyl dimethyl silane hydroquinone) and MTBDMSH (mono-tertiary butyl dimethyl silane hydroquinone) were obtained in 60 and 40% yield, respectively (Scheme 2).

HQ releases H^+ in a basic chemical environment induced by imidazole, a planar five membered ring with vibrant electronic shifts, because hydrogen binds to one of its nitrogen atoms (Scheme 4). Imidazole with 3.67 debye is water soluble.

This mechanism leads to covalent bond formation, which is further broken by hydrolysis.

Imidazole being amphoteric acts as an acid and a base, where an acidic proton is bound to the nitrogen, which deprotonates to form an imidazole anion. The basic site is the nitrogen with a lone pair (and not bound to hydrogen). Its protonation produces the imidazolium cation (Scheme 5). DMAP being basic acts as a nucleophilic catalyst for hydrosilylations with efficient kinetic resolution for phenolic –OH groups (Scheme 5).

Structure: ^{1}H-NMR (500 MHz, $CDCl_3$) δ: 0.19 (s, 6H), 1.00 (s, 9H), 6.72 (m, 4H). ^{13}C-NMR (126 MHz, $CDCl_3$) δ: −4.41, 18.27, 25.82, 116.22, 120.97, 149.26, 149.84.

2.2.2. Deprotection of MTBDSH. Mixtures of DTBDMSH and MTBDMSH (1 mM) silyl ethers and *n*-$Bu_4NF\cdot 3H_2O$ (tertiary-*n*-butyl ammonium fluoride: TBAF) (0.5 mM) in dry THF were stirred at 0 °C for 1 h (Scheme 6). The fluoride of TBAF is a hydrogen bond acceptor and its salts get hydrated with limited solubility in organic solvents. TBAF enhances the solubility of both DTBDMSH and MTBDMSH in this reaction and catalyzes their hydrolysis.

The mixture was evaporated, and the residue was collected in ethyl acetate and washed with saturated $NaHCO_3$ and finally with brine. The residue was purified by flash chromatography with hexane and ethyl acetate in a 4 : 1 ratio to get a colorless solid. TBAF maintains solubilization of the reacting species. The $3H_2O$ of *n*-$Bu_4NF\cdot 3H_2O$ seems to facilitate the hydrolysis of these silyl ethers through bifluoride (HF_2^- or H^+) and hydroxide (OH^-), as well as fluoride. Silyl ethers are hydrolyzed in THF, an aprotic solvent with 7.6 debye. It moderately dissolves *n*-$Bu_4NF\cdot 3H_2O$, DTBDMSH, and MTBDMSH. It is water-miscible for hydrolysis of both DTBDMSH and MTBDMSH for better hydrolysis at RT. The structure to understand the role of TBAF in the reaction mechanism is given below.

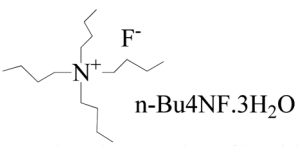

Tertiary-n-butylammonium fluoride-TBAF

Silyl ethers protect groups from alcoholic or phenolic OH in organic synthesis as they combine with different groups for

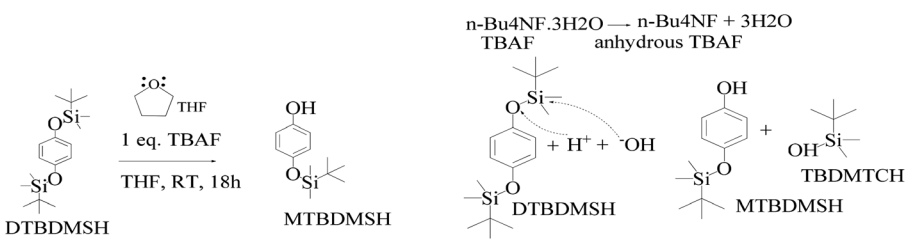

Scheme 6 DTBDMSH deprotection mechanism to MTBDMSH and the dehydration mechanism of *n*-$Bu_4NF\cdot 3H_2O$ to assist MTBDMSH formation.

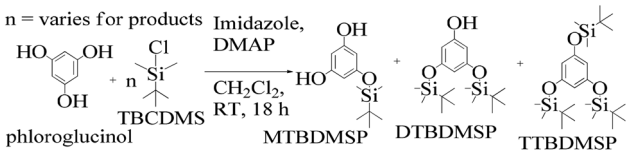

Scheme 7 The phloroglucinol and TBCDMS mechanism in DMAP and CH_2Cl_2 medium at RT for preparing MTBDMSP and other species in small amounts.

a number of silyl ethers. Ether groups provide selectivity for protecting group chemistry. Trimethylsilyl (TMS), *tert*-butyldiphenylsilyl (TBDPS) and *tert*-butyldimethylsilyl (TBDMS) are silyl ethers which are installed and removed very selectively under mild conditions.

2.2.3. Phloroglucinol (1,3,5-trihydroxy benzene) protection. As shown in Scheme 7, imidazole (3 eq.) and DMAP (0.06 g, 0.5% eq.) were added to phloroglucinol solution (1 eq., 6.30 g) prepared in dry DCM (50 ml). TBCDMS solution (2 eq.) was prepared in DCM (20 ml), and was added to the phloroglucinol mixture and stirred for 24 h @ 700 rpm. This reaction was stopped by adding brine (100 ml), which formed aqueous and organic liquid–liquid layers. The aqueous layer was further extracted with DCM (3 × 50 ml), and the total organic phase liquid was dried over anhydrous Na_2SO_4 and evaporated under vacuum. The residue was purified with flash chromatography using a hexane and ethyl acetate mixture in a 4 : 1 ratio and a colorless solid (61%) was collected. Imidazole and DMAP assist safer protection of the phloroglucinol with silyl ethers. MTBDMSP (mono-tertiary butyl dimethyl silane phloroglucinol), DTBDMSP (di-tertiary butyl dimethyl silane phloroglucinol) and TTBDMSP (tri-tertiary butyl dimethyl silane phloroglucinol) were obtained with >90% TTBDMSP.

Therefore, a unique mathematical representation of the participating molecules could be presented as follows:

$$\mathrm{P} + n\mathrm{TB} = (n-1)\mathrm{MT} + (n-2)\mathrm{DT} + (n-3)\mathrm{TT}$$

P is phloroglucinol, TB is TBCDMS, MT is MTBDMSP, DT is DTBDMSP, TT is TTBDMSP, n is the initial moles of TBCDMS, and $(n-1)$, $(n-2)$ and $(n-3)$ are the number of moles of MTBDMSP, DTBDMSP, and TTBDMSP, respectively. It is an addition reaction, so applying reaction kinetics, their $(1-(1/n))$, $(1-(2/n))$, and $(1-(3/n))$ numbers of moles are calculated as:

$$\text{Number of moles} = \frac{[(n-1)\mathrm{MT}]}{[n\mathrm{TB}]}$$

Since TBCDMS and MTBDMSP interact in a 1 : 1 ratio, the stoichiometry for MTBDMSP could be considered as:

$$\text{Stoichiometric ratios} = \frac{[(n-1)]}{[n]} = \left[\frac{n}{n} - \frac{1}{n}\right] \text{ or } \left[1 - \frac{1}{n}\right]$$

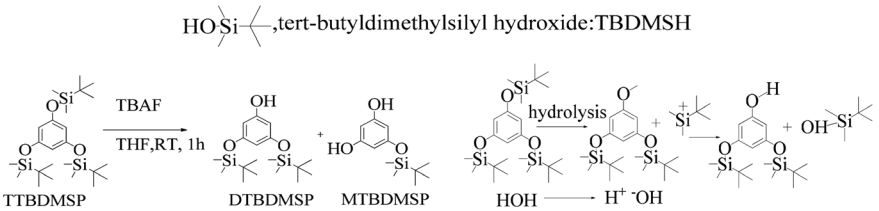

Scheme 8 The TTBDMSP deprotection mechanism in the prescribed medium to prepare MTBDMSP and other species in small amounts at RT.

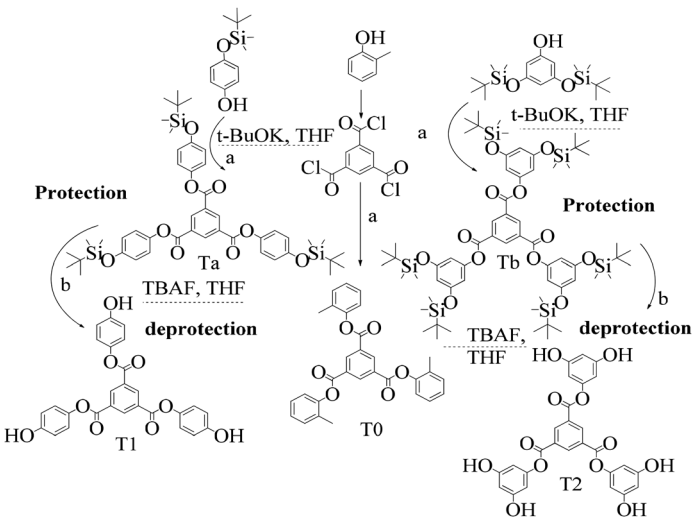

Scheme 9 Brief illustration of 1st tier dendrimer synthesis: (a) *t*-BuOK, THF; (b) TBAF, THF.

Similarly, the number of molecules calculated for DTBDMSP and TTBDMSP is:

$$\text{Numbers of the moles} = \left[1 - \frac{2}{n}\right] \text{ and } \left[1 - \frac{3}{n}\right]$$

Structure: ^{1}H NMR (500 MHz, $CDCl_3$) δ: 0.18 (s, 6H), 0.96 (s, 9H), 4.73 (s, 1H), 5.94 (s, H) 5.98 (s, 2H). ^{13}C NMR (126 MHz, $CDCl_3$) δ: −4.28, 18.34, 25.79, 101.32, 105.24, 156.95, 157.41. HR-MS (CH_3CN) + (m/z) found: 354.3447; calc value for $C_{18}H_{34}O_3Si_2$: 354.2046.

2.3 DTBDMSP deprotection

As shown in Scheme 8, a mixture of the silyl ether of TTBDMSP (tri-tertiary butyl dimethyl silane hydroquinone) (1 mM) and n-$Bu_4NF\cdot 3H_2O$ (0.3 mM) in dry THF was stirred @700 rpm for 1 h at 0 °C. The n-$Bu_4NF\cdot 3H_2O$ catalyzed the hydrolysis of TTBDMSP to get DTBDMSP and MTBDMSP. The solvent is evaporated, and the residue was collected in ethyl acetate. It was washed with dilute HCl, then saturated $NaHCO_3$ and finally with brine. The residue was purified by flash chromatography using hexane and ethyl acetate in a 4 : 1 ratio for the solid product. TBAF catalyzed the hydrolysis of the silyl ethers at RT in a sequential manner. Three times *tert*-butyldimethylsilyl hydroxide was also obtained as a byproduct.

2.4 1st generation dendrimer preparation

A 1 mM solution of MTBDMSP, DTBDMSP or TTBDMSP (3.2 equiv.) phenolic derivative and 2-methylphenol separately and *t*-BuOK base (3.1 equiv.) in dry THF (10 ml) were prepared. 1 equiv. TMC solution in THF was also prepared and added to the PD solutions separately at RT. The contents were vigorously stirred @700 rpm and the reaction was monitored with TLC. The brief mechanism is depicted in Scheme 9.

2.4.1. Tri-*o*-tolyl-benzene-1,3,5-tricarboxylate (TOBT (T0)). A solution of *o*-cresol or 2-methylphenol (3.1 mM, 335.23 mg) and *t*-BuOK (3.1 mM, 347.8 mg) was prepared in 5 mL of THF. A TMC (1 mM, 265.48 mg) solution was also prepared in THF and was added to the *o*-cresol solution dropwise with stirring at 700 rpm at RT for 18 h until all of the TMC was used, as indicated by TLC. The reaction was quenched by adding ice. The water insoluble products were filtered out using a Büchner funnel and a white solid was produced with 85% yield (Scheme 9).

Structure: R_f 0.75 (25 : 75: EtOAc : *n*-hexane); ^{1}H NMR (500 MHz, $CDCl_3$): δ 9.29 (s, 3H), 7.25 (m, 13H), 2.28 (s, 9H) ppm; ^{13}C NMR (125 MHz, $CDCl_3$): δ 163.29, 149.38, 136.27, 131.59, 131.38, 130.33, 127.39, 126.77, 121.95, 16.53. HR-MS (CH3CN) + (m/z) found: 480.9243; calc. value for $C_{30}H_{24}O_6$: 480.1573.

2.4.2. Tris(4-((*tert*-butyldimethylsilyl)oxy)phenyl) benzene-1,3,5-tricarboxylate (Ta). The synthesis process is explained in Scheme 9. A MTBDMSM (3.1 mM) and *t*-BuOK (3.1 mM) solution was prepared in 5 mL of THF. TMC (1 mM) was also prepared in THF and added to the MTBDMSM solution drop-by-drop with stirring at 700 rpm at RT for 18 h until all of the TMC was used, as shown with TLC. The reaction was quenched with cold water and a white solid product was filtered out with a Büchner funnel with 80% yield.

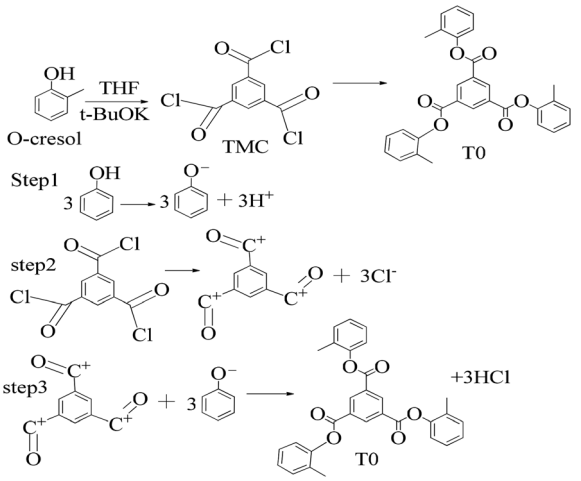

Scheme 10 Synthesis of tri-*o*-tolyl benzene-1,3,5-tricarboxylate (T0) in the prescribed medium in three steps at RT.

Structure: R_f 0.75 with an EtOAc and hexane mixture in 20 : 80 ratio. **Ta** was used to synthesize **T1** as such (Scheme 9). ^{1}H NMR (500 MHz, $CDCl_3$) δ 9.13 (s, 3H), 7.12 (d, J = 8.4 Hz, 6H), 6.90 (d, J = 8.5 Hz, 6H), 1.00 (s, 27H), 0.22 (s, 18H). ^{13}C NMR (126 MHz, $CDCl_3$): δ 163.5, 153.6, 144.4, 135.9, 131.3, 122.1, 120.7, 25.6, and 4.4.

2.4.3. Tris(3,5-bis((*tert*-butyldimethylsilyl)oxy)phenyl) benzene-1,3,5-tricarboxylate (Tb). The synthesis of **Tb** is shown in Scheme 12a. A solution of *o*-cresol (3.1 mM) and *t*-BuOK (3.1 mM) was prepared in 5 mL of THF. A TMC (1 mM) solution was prepared in THF and added dropwise to the *o*-cresol solution. It was stirred at 700 rpm for 18 h at RT, and the reaction was monitored with TLC. The reaction was quenched by adding water and a white product was filtered out with a Büchner funnel with 80% yield. **Tb** was used as such to synthesize **T2**.

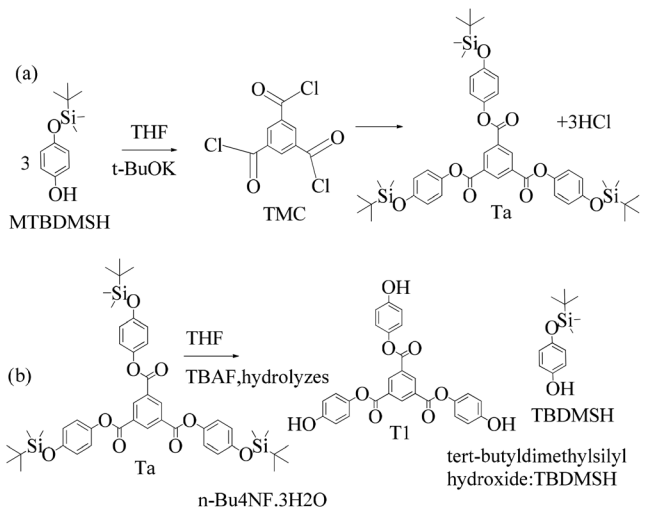

Scheme 11 (a) and (b) Synthesis of tris(4-hydroxyphenyl) benzene-1,3,5-tricarboxylate (T1) in the prescribed medium at RT.

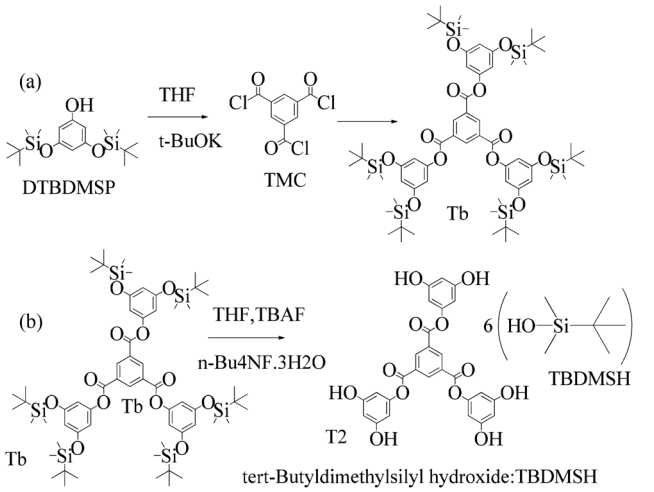

Scheme 12 (a) and (b) Synthesis of tris(3,5-dihydroxyphenyl)benzene-1,3,5-tricarboxylate (T2) in the prescribed medium at RT.

Structure: R_f 0.75 ^{1}H NMR (500 MHz, $CDCl_3$) δ 9.13 (s, 3H), 6.40 (s, 6H), 6.29 (s, 3H), 0.98 (s, 54H), 0.23 (s, 36H); ^{13}C NMR (126 MHz, $CDCl_3$) δ 4.29, 25.76, 29.85, 107.28, 110.33, 131.25, 136.23, 151.64, 157.12, 163.19.

2.4.4. Tris(4-hydroxyphenyl) benzene-1,3,5-tricarboxylate (T1). The synthesis of **T1** is shown in Scheme 11b. A mixture of **Ta** (1 mM) and TBAF (3.1 mM) in dry THF was stirred at 0 °C for 1 h. The solvent was evaporated and the residue was purified by flash chromatography using DCM and methanol in a 9.5 : 0.5 ratio to get a white solid (90%).

Structure: ^{1}H NMR (500 MHz, DMSO) δ 9.61 (s, 3H), 8.84 (s, 3H), 7.13 (d, J = 8.0 Hz, 6H), 6.82 (d, J = 8.0 Hz, 6H); ^{13}C NMR (125 MHz, DMSO): δ 163.63, 155.48, 142.54, 134.63, 130.67, 122.60, and 115.76. HR-MS (CH_3CN) + (m/z) found: 487.1025; calc. value for $C_{27}H_{18}O_9$: 487.0951.

2.4.5. Tris(3,5-dihydroxyphenyl) benzene-1,3,5-tricarboxylate (T2). As shown in Scheme 12b, a mixture of **Tb** (1 mM) and TBAF (6.1 mM) was prepared with dry THF and stirred at 700 rpm at 0 °C for 1 h, and was evaporated. A white solid (85%) was purified by flash chromatography using DCM and methanol in a 9 : 1 ratio.

Structure: ^{1}H NMR (500 MHz, DMSO) δ 9.69 (s, 6H), 8.81 (s, 3H), 6.15 (s, 6H), 5.76 (s, 3H). ^{13}C NMR (126 MHz, DMSO): δ 158.99, 151.88, 144.15, 134.78, 131.76, 100.49, 100.17. HR-MS (CH_3CN) + (m/z) found: 535.0872; calc. value for $C_{27}H_{18}O_{12}$: 535.0798.

Efficient and facile methods for the synthesis of trinuclear Schiff base ligands derived from chiral aminoalcohols were reported elsewhere using vanadium catalysts, but these are altogether different studies. Our study is focused on using free –OH groups to release H^+ ions to scavenge free radicals in a safer manner. Thereby, the protection and deprotection routes were adopted in very simple chemical processes without using any metallic catalyst. The rate of release of H^+ is significant to scavenge free radicals. In this context, **T1** and **T2** dendrimers have been proven very effective within the standard norms of antioxidant activities.[21]

3. Results and discussion

3.1 Characterization

3.1.1. Characterization of the branching unit. ^{1}H and ^{13}C NMR spectra of mono-protected hydroquinone and di-protected phloroglucinol MTBDMSP, DTBDMSP, and TTBDMSP PDs formed with TBDMSCl (*tert*-butyldimethylsilyl chloride)silyl ether were used to elucidate their structures. Side products were used to synthesize the branching unit of the dendrimers with TBAF reagent. In Fig. S4,† mono protected hydroquinone produced two peaks for (9H) of –CH_3 at 1.00 ppm and (6H) of –CH_2 at 0.19 ppm. Phloroglucinol (Fig. S6†) shows 2 peaks for –CH_3 (18H) at 0.96 ppm and for –CH_2 (12H) at 0.18 ppm on silyl ether bond formation. This implies a selective protection of hydroquinone and phloroglucinol (Schemes 9 and 10).

3.1.2. Characterization of the dendrimers. ^{1}H and ^{13}C NMR of **Ta**, **Tb**, **T0**, **T1** and **T2** predicted structures on deprotection of the silyl ether from the dendrimer using TBAF. **Ta** produced 2 peaks for hydroquinone benzene attached to TMC at 6.9 ppm (6H) and 7.1 ppm (6H). This split is caused by hydrogen environments b and c, respectively (Fig. S9†). Peaks d at 0.22 ppm for (18H) and e at 1.00 ppm for (27H) imply silyl ether formation on mono protected hydroquinone bonded to TMC from 3 sides. **Tb** depicted in Fig. S11† produced peaks b at 6.40 ppm and c at 6.28 ppm for (6H) and (3H) of phloroglucinol respectively with peaks d at 0.23 ppm for (36H) and e at 0.98 ppm for (54H). This implied silyl ether formation with phloroglucinol and TMC at 3 sides. In Fig. S1,† **T0** has a peak at (9H) for –CH_3 attached to *o*-cresol at 2.28 ppm and (3H) for the benzene ring core at 9.29 ppm, predicting its structure. The H proton is attached to the c position of the dihydroxybenzene, which has –OH functional groups bonded or attached to the subsequent carbon atoms at both sides of the H at the c position of the **T2** dendrimer (Fig. SI3†). This arrangement develops a unique electron interactive cloud. These H attached to the c position did not produce a sharp peak but developed a visible split in the chemical shift of this H atom. Thus, it depicts that the chemical shifts or the electronic clouds of the H attached to the c position are influenced by the electronic clouds of the H atoms of both the –OH groups. The O atoms of both the –OH groups have two lone pairs of electrons (LPEs) which not only influence its own H electronic clouds but also the spinning of the H in the c position. There may be a possibility that the H at the c position has developed an association with the O atom of the –OH groups through weaker hydrogen bonding, which might have developed a stable spinning. The H of the c position is equally attached by these two –OH groups. Thus, the association could have been equilibrated with a specific electron density of the electronic clouds. This is the reason that the prominent chemical shielding occurs at 6.15 ppm with the 5.60-I integrated area. Also, the d position of the H of –OH is weakly shielded and resolved at 9.69 ppm. Thus, the H atom at position c has a special role. It is chemically not in insolation, but is in an interactive mode with the electronegative O atom of the –OH of the d position. These linkages of the H of the c position fall at 6.15 ppm, so it might assist the release of H^+ from these two

–OH groups, along with chemically equilibrating with the –OH stretching and the spinning in ^{1}H NMR. This is also proven by the fact that the chemical shift of the H^+ placed at the b position (a similar position to that in **T2**) *vis-à-vis* a single –OH group nearby develops a single closely placed sharp split in **T1** (Fig. S13†) as compared to **T2**. Of course, there is a split, but this split is very sharp compared to **T2**. Thus, the chemical shift of the H atom cloud acts as a sensor to distinguish the presence of one –OH or two –OH groups. Similarly, it could also be effective to identify the presence of other functional groups. The H split could also define the chemical activities like hydrogen bonding, LPE, and others.

The **Ta** and **Tb** were deprotected and the peaks for silyl ether were absent in **T1** and **T2**, predicting the structures. The mass spectra of **T0**, **T1**, and **T2** implied the structures. **T0** with larger pi conjugation and effective delocalization of the terminal phenyl groups, core, and LPE of the O atoms of its ester groups is optically active compared to **T1** and **T2**. The dendrimers are insoluble in water and their solutions were prepared in organic solvents. **T0** was dissolved in acetone, while **T1** and **T2** were dissolved in methanol for the optical activities study. They were mixed with DPPH free radicals. **T1** and **T2** were also mixed with aqueous solutions of BSA and lyso at RT. The DPPH solution was prepared in methanol. **T0** did not scavenge free radicals, while **T1** and **T2** both scavenged them. Such experiments are of significance as free radicals initiate undesired activities in biological and biochemical processes. The radicals are highly energetic and interact with proteins, enzymes, and other sensitive biomolecules in cells. **T1** and **T2** acted as biocompatible sensors as they scavenged free radicals and bound the proteins.

T1 and **T2** with 3 and 6-OH acted as flavonoids to detect DPPH (1,1-diphenyl-2-picrylhydrazyl) free radicals and scavenge them. **T1** and **T2** have aggregated BSA and lyso in their void spaces, which decreases their antioxidant activities compared to ascorbic acid as a standard antioxidant. The free radical scavenging kinetics for 25 μM (micromol L^{-1}) to 1 mM (millimol L^{-1}) **T1** and **T2** were investigated separately with DPPH at RT using UV-Vis spectrophotometry. This determined the efficient concentration (EC_{50}) of **T1** and **T2** for DPPH radical scavenging calculated from UV-Vis absorption. **T1** and **T2** have 0.424 and 0.04312 mM EC_{50} values, respectively, and quickly scavenged radicals. **T2** induced comparatively stronger electronic activities than **T1** by acquiring more activation energy. The BSA and lyso

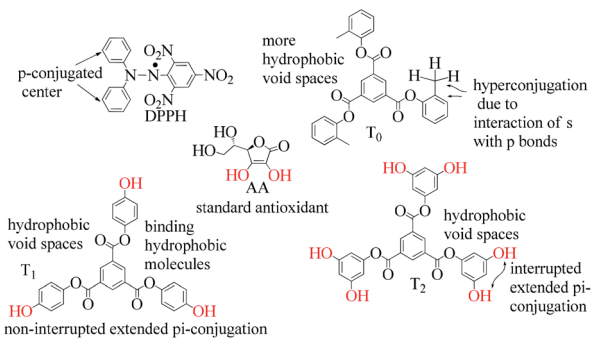

Fig. 1 Structures of DPPH, AA, T0, T1, and T2.

concentrations were studied separately and found to be 0.424 and 0.04312 mM for **T1** and **T2**, respectively. The binding of more BSA than lyso may be due to the fact that the BSA preferred entering the void spaces due to the hydrophobic environment of the void spaces.

3.1.3. Proton H^+ releasing activities. Di- and trihydroxybenzene branches have active sites due to LPE and π conjugation with interactive activities.[21,22] Antioxidant abilities are evaluated with a DPPH assay[23] using ascorbic acid (**AA**). The EC_{50} values of **T1** and **T2** with BSA and lyso were studied.[24,25] From **T0**, **T1**, and **T2**, the π-conjugation area is widened to aggregate smaller as well as larger sized FRs to scavenge. EWG (electron releasing group, $-CH_3$) and π-conjugation constituents generated nucleophilic and electrophilic activities of the void spaces for sensing FRs. Carboxylic ($-\overset{O}{\overset{\|}{C}}-O-$) constituents as the linker, phenyl as the branches, and $-CH_3$ with **T0**, 1-OH with **T1** and 2-OH with **T2**, respectively, induced hydrophobicity in the structures, as shown in Fig. 1. The –OH groups shown in red have H^+ releasing ability.

T0, **T1**, and **T2** can bind greasy hydrophobic waste materials due to hydrophobic interactions. **T0** with electron releasing 3-CH_3 attached to its terminal phenyl group acted as a superhydrophobe as it is not soluble in methanol (CH_3OH) but is soluble in acetone $(CH_3)_2CO$. **T1** and **T2** were dissolved in methanol, which indicated interaction of phenolic –OH and alcoholic –OH groups. **T0** initiated hyperconjugation due to its sigma bond activities of the H atom of the $-CH_3$ with the pi bond of the terminal phenyl. It adsorbed more UV/Vis light than **T1** and **T2**. **T0**, **T1**, and **T2** have H^+ releasing 0, 3, and 6-OH respectively (Fig. 2) with scavenging activities.

3.1.4. BSA and lysozyme. Radicals vibrantly interact with protein, DNA, enzymes, and hormones.[26] Proteins and enzymes sensitively respond to pH, H^+ ions and others due to alpha and beta sheet deconvolution. BSA has 583 amino acids with 17 disulfide bonds and 1 free cysteine group that initiate interactions with dendrimers.[26,27] BSA crosslinks with –OH radicals in the absence of oxygen[28] while in the presence of oxygen, an alteration of protein size occurs to a limited extent.[24] **T0**, **T1** and **T2** aggregate BSA in their void spaces through an affinity with π conjugation, EWG, and LPE of the voids. BSA at 66 kDa and lyso at 14.3 kDa consist of 583 and 129 amino acids, respectively, and BSA aggregates in the voids but lyso get distributed in the solution. Liu *et al.* have described antioxidant fractions of lyso hydrolyzate.[29] The –OH of **T1** and **T2** release H^+, which develops a nucleophilic O^- to generate phenyl as well as –OH equilibrium.[30]

3.1.5. Free radical scavenging activity measurements. The DPPH· scavenging capacity of the dendrimers was measured with a Brand-Williams assay.[23] 300 μM DPPH solution was prepared in methanol and kept in the dark to prevent photocatalytic activities. **T1** and **T2** stock solutions were separately prepared in methanol. **T0** was not soluble in methanol so its solution was prepared in acetone. BSA and lyso solutions were prepared in water, and DPPH solution was prepared in methanol. A 2.5 ml volume containing 1 ml DPPH (300 μM) + 0.5 ml aq-BSA or lyso (separately) + 1 ml dendrimer solution in variable concentrations was used for the experiment. Variable

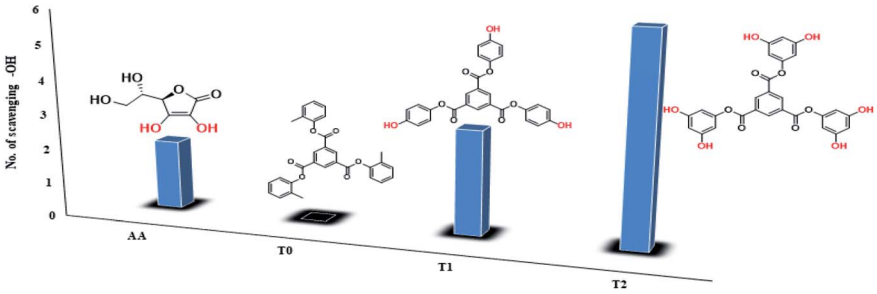

Fig. 2 Number of –OH groups and DPPH free radical scavenging activities.

dendrimer concentrations were added to fresh DPPH· solution from 25 to 1000 μl and the mixture was shaken at 200 rpm for 1 min to form a homogeneous suspension. UV/Vis absorption at 520 nm was recorded at a fixed time interval. The % DPPH scavenging was determined with the following equation:

$$\%\ \text{DPPH scavenging} = \%\ \text{EC} = \left(\frac{A_o - A_t}{A_o}\right) \times 100 \quad (1)$$

A_0 is initial absorbance and A_t is the absorbance of the mixture at the chosen time interval at 520 nm. EC_{50} is the concentration needed to scavenge 50% DPPH at RT. The time to reach a steady-state at EC_{50} is termed as TC_{50}. Antioxidant efficacy (AE) by combining both the EC_{50} and TC_{50} factors is calculated using eqn (2).

$$\text{AE} = \frac{1}{\text{EC}_{50} \times \text{TC}_{50}} \quad (2)$$

The scavenging capacities of **T1** and **T2** compared to ascorbic acid as a standard are evaluated.

3.1.6. Kinetic studies of the scavenging reaction. Under similar experimental conditions, the dendrimers interacted with DPPH· through two steps (Fig. 3). Initially, the DPPH· concentration compared to **T0**, **T1**, and **T2** was in excess but it was reduced with time linearly. The rate constant (k) for scavenging DPPH is written as:[31]

$$[\text{A}] = [\text{A}]_0\, e^{-kt} \quad (3)$$

The k values are calculated from the slopes of the UV/vis abs *versus* time plot. The DPPH concentration [A] left after time t s is determined from UV abs. The initial DPPH $[A]_0$ concentration is known. The scavenging kinetics of DPPH with time ascertained its order. The Gibbs energy (ΔG, J mol^{-1}) is determined for the scavenging activities of **T0**, **T1** and **T2** at RT. ΔG is calculated using the equation:[32]

$$\Delta G = -2.303\text{RT}\log(A/A_0) \quad (4)$$

A and A_0 are the absorptions of the sample at 0 min and after 270 min, respectively. These are directly proportional to the DPPH concentration at the respective time.

3.2 Scavenging activities and kinetics of the dendrimers

The lowering of the UV/Vis absorption with DPPH on increasing the dendrimer concentration implies a significant DPPH scavenging (Fig. 5). The EC_{50} for the dendrimers is determined compared to the standard **AA**. Increasing the dendrimer concentration increased the scavenging activities depending on the individual amount of **T0**, **T1**, and **T2**. DPPH scavenging depends on the H^+ releasing ability of the dendrimers. A H^+ ion accepts the extra electron of DPPH and develops a –N–H covalent bond by reduction. The scavenging ability increases on increasing their concentrations because the number of –OH also increases, but despite the release of H^+, their pH remains constant. **T1** and **T2** act as a buffer with adequate DPPH amount as the released H^+ is directly engaged in FR scavenging without affecting the pH. This is a novelty of **T0**, **T1** and **T2**. The moment they release H^+, it is used by an unshared electron on the N atom of DPPH. The H^+ release is balanced by a delocalization of the phenyl or benzene ring. **T0** has 3 terminal phenyl groups containing one $–CH_3$ each. **T0** does not have –OH so no H^+ is released and no free radical scavenging occurred. **T0** is similar to TTDMM reported in our previous work, but it has delocalization in the branching contrary to **T0**, so it can encapsulate the drug silibinin. **T1** with 3-OH and **T2** with 6-OH scavenged

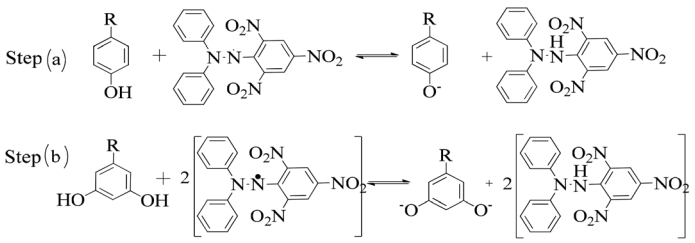

Fig. 3 (a, b) Interacting activities of the dendrimers with DPPH radicals in two steps. Step (a) occurs when the ratio of dendrimer to DPPH is 1 : 1, while step (b) occurs with a 1 : 2 ratio according to the H^+ holding ability of the PDs to decide the rate constant.

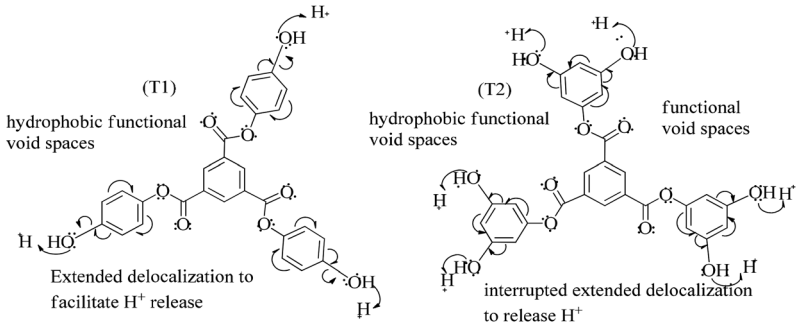

Fig. 4 H^+ releasing activities of T1 and T2 to scavenge DPPH radicals.

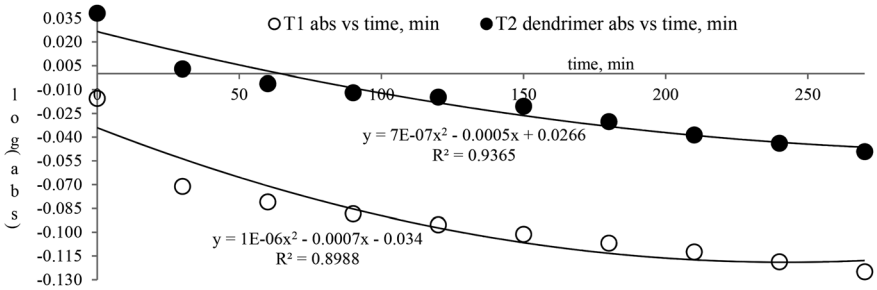

Fig. 5 Abs *vs.* time of T1 and T2.

DPPH by 94 and 92%, respectively, at 0.424 and 0.4312 mM respectively. **T1** and **T2** release 3 and $6H^+$, respectively, but **T1** with 50% less H^+ scavenged FRs by 2% more than **T2**. The H^+ releasing action of **T1** is stronger than that of **T2**, due to an interruption as 2-OH are placed at the *meta* position of benzene. Such interference occurs due to electron–electron interactions among their LPEs, which is missing in **T1**. **T0** contains a H atom in TMC as well as in the terminal benzene rings and $-CH_3$, but no H^+ was released. **T1** and **T2** have detected H^+ release. **T1** and **T2** have H^+ releasing –OH so they tune their electron delocalization. The H^+ releasing activities of **T1** and **T2** are controlled by their extended delocalization. **T1** produced 94 and **T2** produced 92% scavenging. The rate of release and use of H^+ should have been equal but release required some activation energy due to interrupted delocalization as is noted in Fig. 4. The –OH with 2 LPEs on the O atoms initiate electron withdrawing activities from the benzene rings of **T1** and **T2**, where **T1** facilitates expeditious H^+ release without any interruption. So **T1** does not undergo any electronic reorientation contrary to **T2**. It faces interruption due to another –OH as it also initiates extended conjugation. It needs comparatively more activation energy as it has a comparatively higher potential energy (Fig. 4). The activation energies of **T1** and **T2** are **T2** > **T1** with frequency factor A being **T1** > **T2**. Abs is a function of time, min, so these data are calculated using the Arrhenius eqn (5).

$$\log \text{abs} = \log A - \frac{E_a}{R}\left(\frac{1}{t}\right) \quad (5)$$

abs is absorption, A is frequency factor or number of collisions, E_a is activation energy, $R = 8.314$ J mol^{-1} K^{-1}, and, t is time in min for abs.

The higher activation energy for **T2** than **T1** implies stronger **T1** spontaneity in releasing H^+ compared to **T2**. This is supported by the higher frequency factor A for **T1**. Regression analysis of the data is given in the equation depicted in Fig. 5 along with the respective plots. The 2-OH of **T2** restricts its number of collisions compared to **T1** because of a localized competitive extended delocalization of both the –OH groups. A weaker H^+ releasing spontaneity is observed for **T2** that required higher activation energy, which could be possible as both the –OH groups may also develop hydrogen bonding. **T2** scavenged DPPH by 92% compared to 94% for **T1**, so the numbers of –OH do not matter to scavenge FRs but their position on the host unit decides their scavenging activities.

Uninterrupted delocalization of **T1** due to $3H^+$ and the presence of $6H^+$ with **T2**, respectively, occurs through electron or delocalization activities. Thus initiating H^+ release as well as scavenging requires energy. On getting the required activation energy, their reorientations tune the nucleophilic and electrophilic sites as per sp^2 to sp^3 electronic transitions through the HOMO (highly occupied molecular orbital) and LUMO (lowest occupied molecular orbital) of **T0**, **T1**, and **T2**. The activation energy requiring activities of these two sites are not equal for **T0**, **T1**, and **T2** and create a hysteresis in their optical activities *vs.* scavenging potential.

T0 among **AA**, **T0**, **T1**, and **T2**, has higher abs due to hyperconjugation as it has electron releasing $-CH_3$ (Fig. 6). A sigma bond of $-CH_3$ and pi bond of phenyl initiate hyperconjugation,

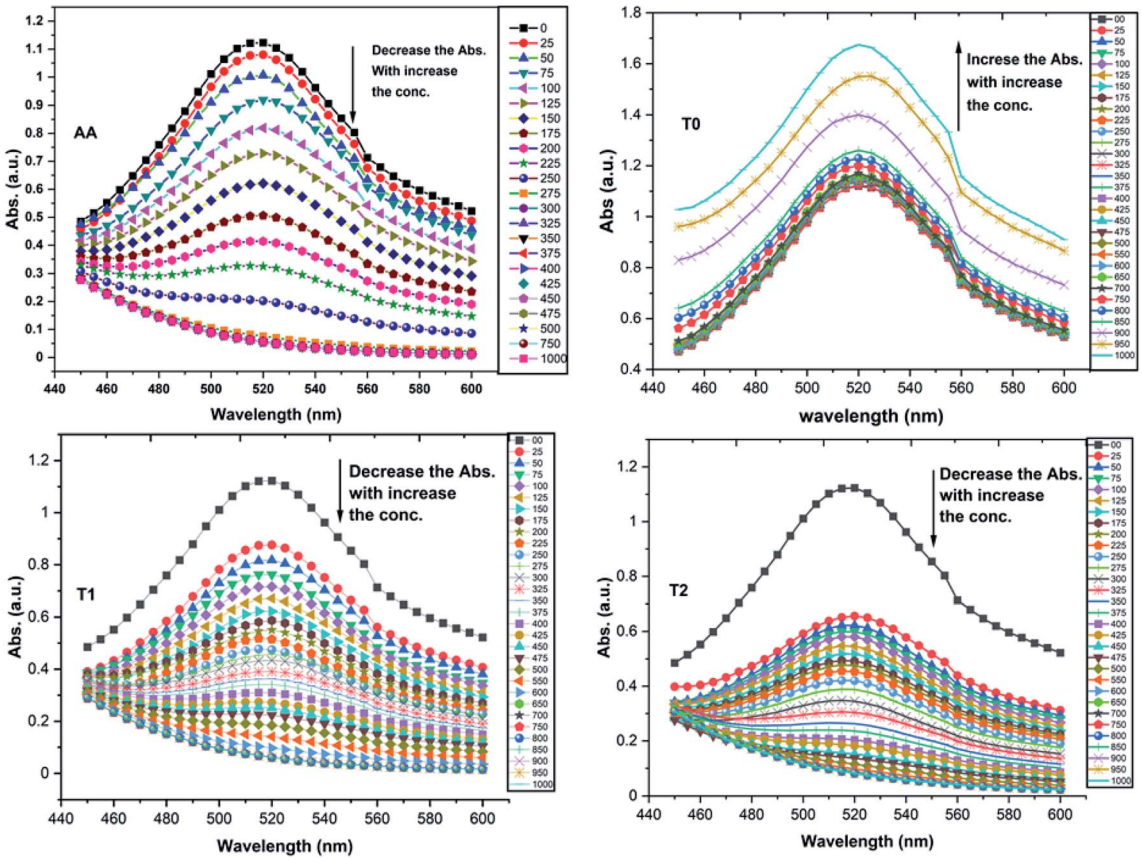

Fig. 6 UV-Vis abs spectra for DPPH radicals with AA (ascorbic acid), T0, T1, and T2.

which detains a larger amount of UV/Vis light. Fig. 6 shows the higher abs with DPPH when **AA** was not added so a larger population of radicals absorb much UV/vis light. On increasing the **AA** concentration in the DPPH solution, the H^+ release simultaneously decreased abs. A single or unpaired electron developed intensified cycles of h^+ and e^- holes, which engage UV light or photons. The H^+ neutralized an unpaired single electron of DPPH and the lowest number of redox cycles occurs. On using H^+, the UV/Vis abs is decreased. The H^+ consumption occurred at a similar λ_{max}. No transitions occur in the structures except for the release of H^+ from **T0**, **T1**, and **T2** and the consumption of the released H^+ by DPPH. Experiments at different pH, and the scavenging activities of **T0**, **T1**, and **T2** are being pursued and will soon be communicated. The H releasing mechanisms of **T1** and **T2** are controlled by their extended delocalization, which induces faster sp^2 to sp^3 electronic transitions on receiving UV/Vis light. **T1** predicted 94% and **T2** 92% scavenging. The rates of release and use of H^+ should have been equal or more for **T2** as it has 2 times more H^+ in its structure. Probably H^+ release requires more activation energy for re-orientation of molecules to match the nucleophilic and electrophilic sites, which requires time. These two events are not equal so a difference occurs in H^+ release and FR scavenging. A linear relationship between abs *vs.* **AA** concentration indicates direct scavenging. A 0.5 mM **AA** stock solution was prepared in MeOH and from 5.0 to 200 μM scavenged DPPH radicals. The **AA** from 5.0 to 55 μM had a reduced transition state due to protonation of DPPH radicals. But 55 μM **AA** stopped responding to UV abs at 520 nm due to complete **AA** oxidization by DPPH radicals getting reduced themselves. The decrease in abs is almost constant on increasing the **AA** concentration (Fig. 7 and 8). The EC_{50} value calculated from the abs *vs.* concentration plot is 32.61 μM. **T0** was dissolved in acetone from 10.0 to 400.0 μM and the abs for **T0** is plotted in Fig. 7. The **T0** undergoes aggregation on increasing its concentration from the initial 10.0 μM. These increments in abs on increasing **T0** concentration largely occur as it does not have electron donating –OH or H^+ releasing groups, so it did not scavenge, rather it gets monodisperse and absorbs visible light at 520 nm from 20.0 to 300.0 μM. **T0** has 3 phenyl groups each with one $–CH_3$, which induce adequate electronic transitions with more UV/Vis light abs. However, after this concentration range with DPPH its abs increased drastically (Fig. 7(A–E)). This shows stability in abs due to saturation in the electronic transitions from HOMO to LUMO. The abs is increased at a certain concentration with a 2nd order mechanism compared to the 1st order interaction of **T1** and **T2**. **T0** activates DPPH to absorb visible light from 10.0 to 300.0 μM with a minor increment. This is not due to radical scavenging but due to π–π interactions. Visible light absorption by **T0** implies activities of π-conjugation of phenyl groups, LPEs of O atoms, and electronic activities

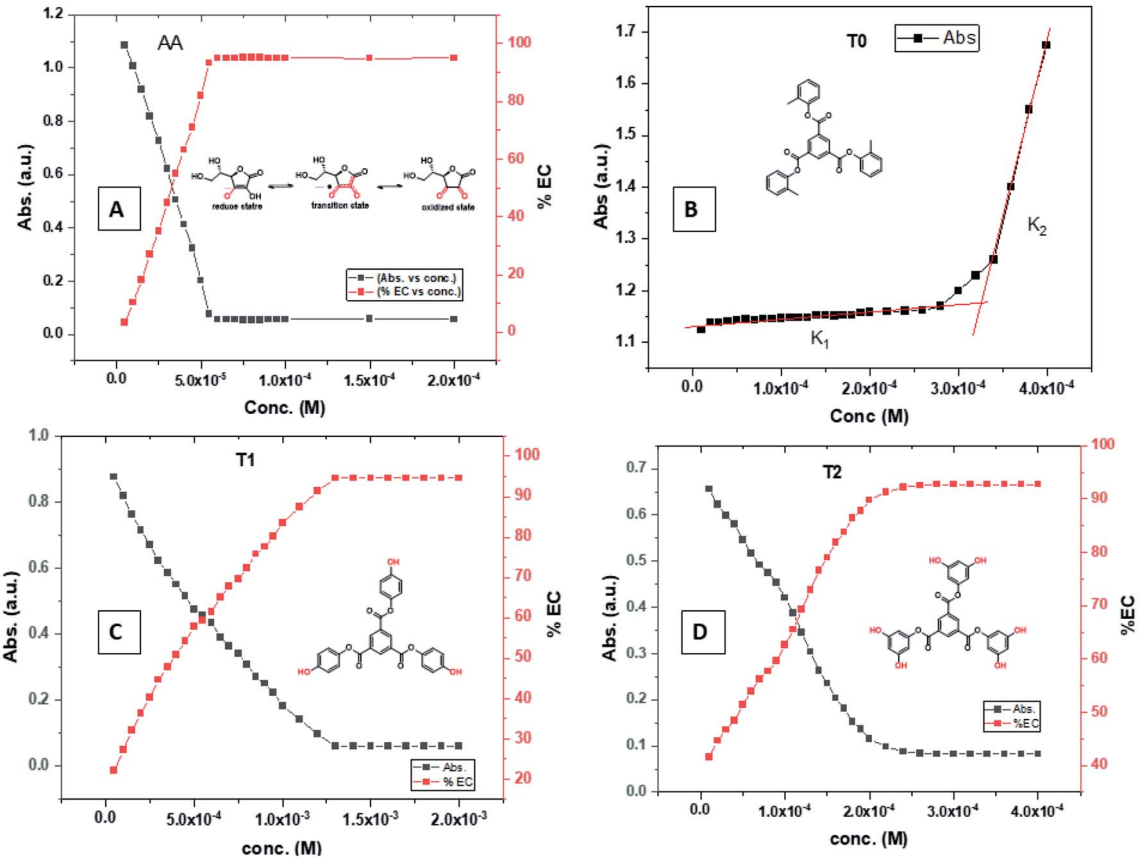

Fig. 7 (A) Abs *vs.* conc. and abs *vs.* % EC of **AA**, (B) abs *vs.* conc. of **T0**, (C) abs *vs.* conc. and abs *vs.* % EC of **T1**, (D) abs *vs.* conc. and abs *vs.* % EC of **T2**.

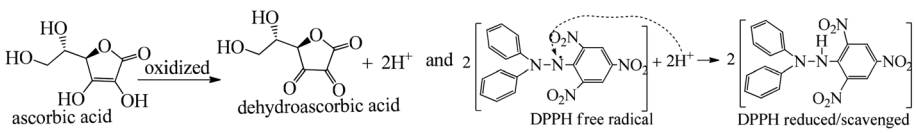

Fig. 8 DPPH scavenging mechanism of ascorbic acid to dehydroascorbic acid.

of its $-CH_3$. These electronic activities imply its structural stability and active optical activities.

The electron releasing $-CH_3$ and benzene ring induce coulombic interaction with **T0** due to intramolecular electronic orientations. Delocalization of the π bond of the terminal phenyl along with ERG develops a negative charge at the center of the phenyl, which may repel DPPH radicals to other energy states. Electron–electron repulsions cause aggregation of **T0**, rather than opting for monodispersion; however, the medium plays a critical role. Acetone tends towards DPPH so after a certain concentration, **T0** undergoes self-aggregation, and UV/Vis implies it as the critical aggregation concentration. Contrary to that, **T0** showed increased abs with concentration, and **T1** and **T2** both showed decreased abs at 520 nm. The decreasing abs rate from **T1** and **T2** changes with concentration due to 3 and 6-OH with **T1** and **T2**, respectively. Abs *vs.* concentration curves of **AA**, **T0**, **T1**, and **T2** are depicted in Fig. 7(A–D); **AA** shows a sharper transition in DPPH scavenging, while **T0** with more UV/Vis abs produces a smooth transition in optical activities at 3.3×10^{-4} M. A higher abs by **T0** occurs due to electron releasing 3-CH_3, due to stronger transition as no part of the abs is lost contrary to **T1** and **T2** which participate in releasing H^+ on absorbing UV/Vis light. **T0** is a robust UV/Vis light absorbent, and it has photocatalyzed the conversion of fluorescent dye methylene blue to colorless leuco methylene blue (Fig. 10A).

The H^+ releasing activity of ascorbic acid is active as its 2-OH undergoes electronic transition to release H expeditiously, contrary to the dendrimers. **T0** did not produce a sharper absorption point on increasing the concentration, but **T1** and **T2** produced a smooth saturation point of abs (Fig. 7A–D). One ascorbic acid reduced 2 DPPH radicals (Fig. 8). Also **T1** and **T2** each have reduced 3 and 6 DPPH radicals, respectively. Fig. 9(A–D) imply free radical reducing kinetics from 0 to 300 min for fixed compositions of radical and of antioxidants under similar experimental conditions. The H^+ release and utilization is in a 1 : 1 ratio.

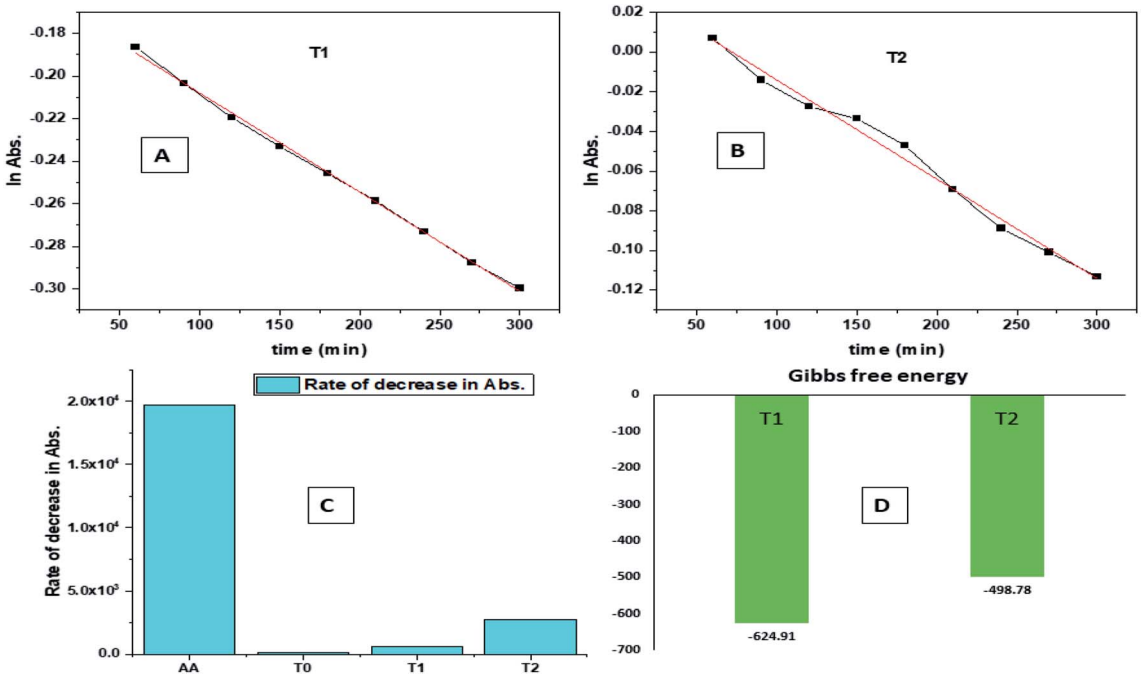

Fig. 9 (A) Time *vs.* ln abs of **T1**. (B) Time *vs.* ln abs of **T2**. (C) Rate of decrease in abs. (D) Gibbs free energy.

The rates of abs by **AA**, **T0**, **T1**, and **T2** decrease. This is supported by Gibbs free energy (Fig. 9A–D). **T2** has higher Gibbs energy with 2-OH, which increases the stability.

The scavenging ability of **T2** is 10 times higher than that of **T1** so the MIC (minimum inhibition concentration) for **T2** is ten times lower than that for **T1**. A single **T2** releases $6H^+$ against $3H^+$ from **T1** (Table 1). This denies a possibility of hydrogen bonding between the two species at a common benzene ring along with a constant effect of π conjugation. **T1** and **T2** follow a straight-line decrease in abs like **AA**, so no generation of a secondary chemical mechanism other than the scavenging activity occurs.

T1 may release H^+ in three steps and scavenge FRs in three steps with three scavenging orders. The 1st H^+ release and scavenging are faster as initially no H^+ exists and no FR was scavenged so dispersion seems active. The 2nd H release could comparatively be lower and a 3rd H release could be lowest. For **T2**, the order to releasing H and scavenging FRs seems to be in 6 steps with subsequent lowering in the H release and scavenge steps. This is one reason that the **T1** scavenging is 10 times faster than that of **T2**.

3.2.1. Electronic transitions. The $-CH_3$ at the *p*-position of the terminal phenyl deshields H of the benzene ring in the core that has stronger optical activities with **T0** > **T1** > **T2** ppm deshielding order (Table 2). The $-CH_3$ electrons by moving towards the terminal benzene influence the LPEs of both O atoms in $3(2n \rightarrow 2\pi^*)$ shifts. n is the number of nonbonding electrons. The $6\pi^*$ transitions further influence the delocalized 3H of TMC, which have undergone higher deshielding with H^1 NMR peaks at 9.29. This decreases on replacing $-CH_3$ with –OH at the *p*-position of benzene. A transition state is induced, which is mathematically formulated as eqn (7).

$$\mathbf{T0} + h\nu \leftrightarrow \mathbf{T0}^*, \tag{6}$$

so

$$k_b = \frac{[T0]}{[T0^*]} \tag{7}$$

The k_b predicts a transition state but after a certain concentration of **AA**, it is stabilized by developing an extreme transition state. Due to the $-CH_3$, the **T0** detains maximum UV/Vis light but it saturates at 2.0×10^{-4} μM as the abs starts increasing with its concentration. The **AA** did not release H^+ causing electronic vibrations and oscillations which get saturated as the **AA**–**AA**–DPPH interactions might have aggregated the DPPH radicals. The abs with **T0**, **T1**, and **T2** distinguishes the H^+ releasing energy (Table 3).

Scavenging efficiency was calculated with eqn (8), and $A_0 = 1.123$ is the abs for DPPH in methanol, whereas the abs A values for **T1** and **T2** at maximum scavenged DPPH sample in methanol.

$$\text{DPPH scavenging activities} = \left(\frac{A_0 - A_s}{A_0}\right) \times 100 \tag{8}$$

Abs values where maximum DPPH was scavenged were used from Fig. 10D and E. The **AA**, **T1**, and **T2** scavenged 95.13, 93.32, and 94.21% DPPH, respectively.

Activation energies and frequency factor and DPPH radical scavenging were calculated fitting abs with Arrhenius eqn (5). The binding or scavenging constant was determined by analyzing the rate of radical scavenging on increasing the

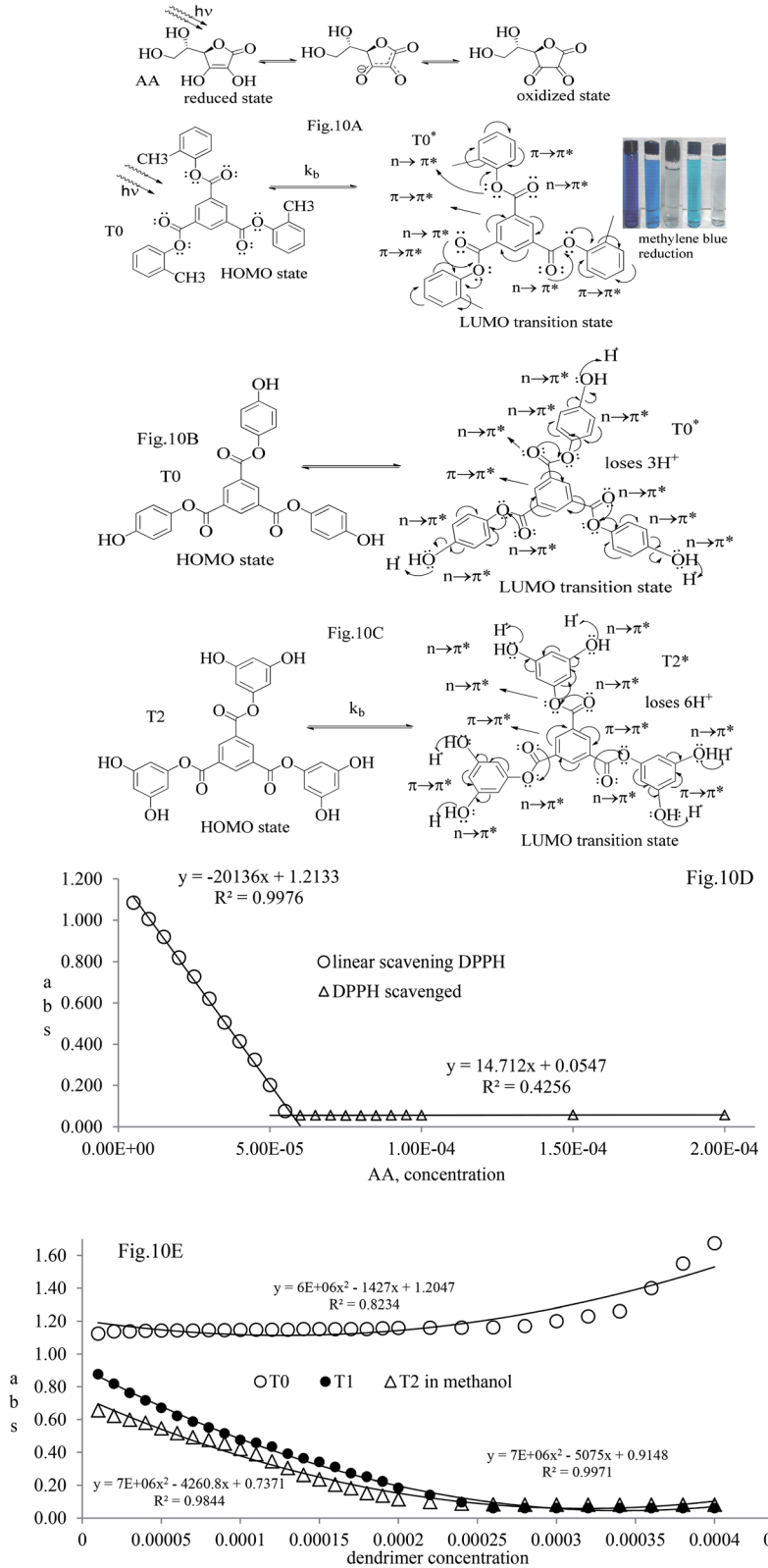

Fig. 10 (A–C) Optical activities from the HOMO to LUMO to scavenge DPPH radicals. (D) Abs *vs.* AA composition with 1st order scavenging of DPPH free radicals. (E) Abs *vs.* dendrimer composition to scavenge DPPH free radicals.

Table 1 Experimental parameters of the phenolic dendrimers

Compound	Scavenging –OH	EC_{50}, M (mol L^{-1})	Max, % EC	TC_{50} (min)	AE	Rate constant (M s^{-1})
T0	0	—	—	—	—	—
T1	3	4.24×10^{-4}	94.57	811.11	5.23×10^{-7}	3.86×10^{-5}
T2	6	4.312×10^{-5}	92.70	945.6	4.56×10^{-8}	4.73×10^{-4}

Table 2 ^{1}H NMR and ^{13}C NMR shifts for H and C of the dendrimers[a]

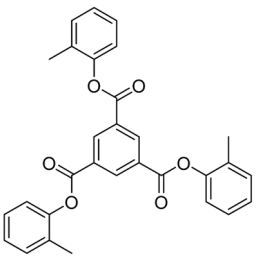
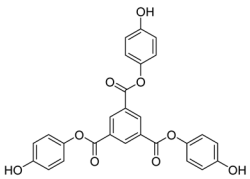
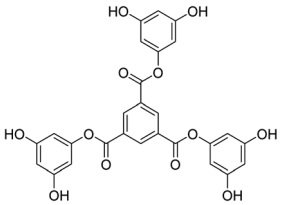

NMR peak	^{1}H	^{13}C	^{1}H	^{13}C	^{1}H	^{13}C
Core benzene	δ 9.29 (s, 3H)	136.27, 130.33	δ 8.84 (s, 3H)	134.63, 130.67	δ 8.81 (s, 3H)	134.78, 131.76
Peripheral benzene	δ 7.25 (m, 12H)	149.38, 131.59, 131.38, 127.39, 126.77, 121.95	δ 7.13 (d, 6H), δ 6.82 (d, 6H)	142.54, 155.48, 122.60, 115.76	δ 6.15 (s, 6H), δ 5.76 (s, 3H)	151.88, 144.15, 100.49, 100.17
Ester bond	—	163.29	—	163.63	—	158.99
$-CH_3$	δ 2.28 (s, 9H)	16.53	—	—	—	—
–OH	—	—	δ 9.61 (s, 3H)	—	δ 9.69 (s, 6H)	—

[a] The $-CH_3$ ERG at the *p*-position of the terminal benzene deshields the H of the benzene ring in the core.

dendrimer composition. These are fitted using the Nernst equation for Gibbs energy determination (Table 3).

$$dG = -nRT \ln k_b \quad (9)$$

The activation energy and scavenging d*G* are correlated with frequency factor. **T2** needs higher activation energy as it has 2-OH, which hinders extending the delocalization of the terminal benzene ring (Fig. 11A). The E_a values listed as **AA** > **T1** > **T2** > **T0** imply that **AA** requires the least energy for releasing $2H^+$, whereas **T0** needs higher activation energy to reach the LUMO from the HOMO (Fig. 11A). **T2** compared to **T1** needs more activation energy than **T1** in releasing H^+.

Net Gibbs energies were determined as follows:

$$\Delta H^+_{releasing} dG = \Delta G\mathbf{T0} - \Delta G\mathbf{T1}$$

$$\Delta H^+_{releasing} dG = -200.484 - 95.866 \text{ J mol}^{-1}, -296.35 \text{ J mol}^{-1}$$

Similarly, for the energy needed to release $2H^+$ from **T2**:

$$\Delta H^+_{releasing} dG = \Delta G\mathbf{T0} - \Delta G\mathbf{T2}$$

$$\Delta H^+_{releasing} dG = -200.484 - 328.378 \text{ J mol}^{-1}, -538.862 \text{ J mol}^{-1}$$

Net d*G* considered from **T0** up to **T2** is higher, partly because it is used in overcoming the hindrance being caused by the extended delocalization activities of its 2-OH on the terminal

Table 3 Frequency factor '*A*', 1st and 2nd order slopes *S* and *S*′, activation energy E_a, J mol^{-1} K^{-1}, scavenging constant k_b and Gibbs free energy d*G*, J mol^{-1}

System	ln *A*	*S*	*S*′	*A*	E_a	k_b	d*G*
AA	8.46×10^{3}	−0.1823	7.00×10^{-7}	0	1.5156	1.2133	−208.142
T0	9.72×10^{-2}	-2.00×10^{-6}	2.00×10^{-11}	1.2508	1.66×10^{-5}	1.2047	−200.484
T1	-1.01×10	0.0002	-1.00×10^{-8}	10.3398	1.66×10^{-3}	0.9148	95.86546
T2	-1.04×10	4.00×10^{-5}	-3.00×10^{-10}	10.9724	3.33×10^{-4}	0.7371	328.3781

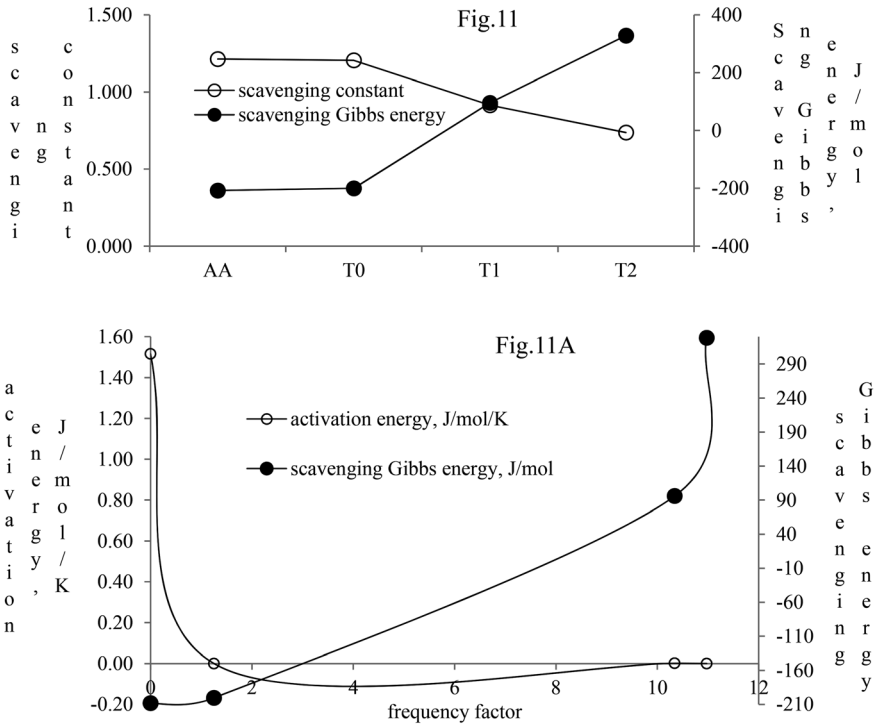

Fig. 11 Scavenging constant and scavenging d*G* of the dendrimers with DPPH radicals. (A) Activation energy and scavenging d*G* with frequency factor.

phenyl group. The activation energy, listed as **AA** > **T1** > **T2** > **T0**, induces a transition either to release H^+ or to undergo a transition state. The abs with increasing concentration is abs**T0** > abs**T1** > abs**T2**, on increasing n → π*, due to, –CH_3, –OH and –2-OH species, respectively. Abs utilizes UV light to initiate HOMO to LUMO state through n → π*, and π → π*. The deshielding patterns of 3H of the core are **T0** > **T1** > **T2** with 9.29 > 8.84 > 8.81 ppm chemical shifts, respectively. The –CH_3 induces stronger deshielding than the others but when –OH are 2-OH exist with **T1** and **T2**, respectively, then they weaken deshielding. This matches with the abs trends, but in a similar way deshielding of ^{13}C is **T2** > **T1** > **T0** with 131.76 > 130.67 > 130.33 ppm, respectively. This implies a high deshielding of **T2** due to 2-OH. NMR and UV/Vis studies implied that the number and nature of the functional groups attached to the dendrimer deshield the core. Hence, a core contributes to the electronic populations. 1-OH to 2-OH of **T1** and **T2** enhances the shielding of H. This initiates H^+ release from –OH and not from the benzene ring. The n → π* population stabilizes the H of the phenyl (Fig. 10A–B). The H of –OH of **T1** and **T2** are deshielded and release with lower abs. The C atom is shielded from **T0** to **T2**. The k_b and d*G* for antioxidants are depicted in Fig. 11A with higher values of k_b implying faster H^+ release activities denoted as:

$$\text{HOMO} + h\nu \xrightarrow{k_b} \text{LUMO} \text{ and } k_b = \frac{[\text{LUMO}]}{[\text{HOMO}]}$$

K_b > 0.5 values depict [LUMO] > [HOMO] transitions and are fitted within the Gibbs energies. Stronger transition implies more LUMO population that decreases the potential energy to convert it into electronic vibrations and oscillations. Fig. 11A depicts lower/higher negative Gibbs energy for higher k_b values. **T2** produced a lower k_b value which utilizes lower energy and has positive d*G* values. A faster [HOMO] species conversion into [LUMO] species needs more energy with d*G* as **T2** > **T1** > **T0** > **AA**. **T2** has lower k_b so the LUMO species are lower for **T2** as electron–electron collisions are hindered.

3.2.2. Role of trimesoyl chloride (TMC)/1,3,5-benzenetricarbonyl trichloride. TMC acted as a core to develop the covalent bonds with phenols used for developing branching around the TMC through its –COCl (carbonyl) groups. The Cl^- of the –COCl is replaceable by the branching molecules to bond with the O atom of the –COCl through the covalent bond. Therefore, the TMC is a workable core and remained stable, so it did not induce any undesired chemical activities during the replacement of the Cl^-. The two electronegative O and Cl atoms of the –COCl group are attached to the core at the same carbon atom of the TMC and can generate competition among the electron attraction towards their own sides. The O atom is a stronger electronegative atom while Cl^- is a mild electronegative atom. Thus, the Cl^- is easily replaced in the chemical process in the presence of the O atom bonded with the carbon atom of the TMC through the double bond. Scheme 1 depicts hydroquinone protection with the TBCDMS to develop the DTBDMSH and MTBDMSH products. Scheme 6 explains its deprotection through silyl ethers and TBAF at 0 °C to produce MTBDMSH. The phloroglucinol protection mechanisms are depicted in Schemes 7 and 8. Now the TMC is used as a core as it has replaceable 3Cl^- anions. Hence, for **T0**, the 2-methylphenol reacted with the Cl^- of the TMC. It is a chemically

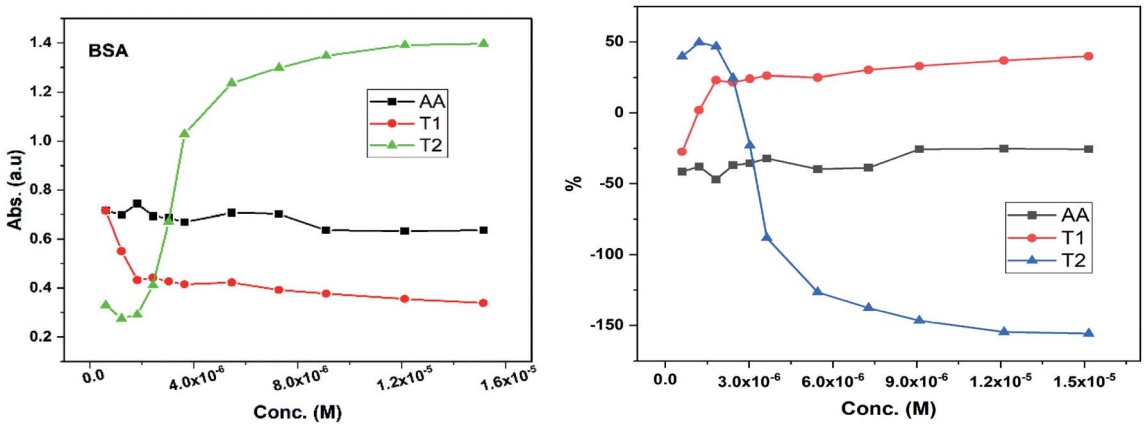

Fig. 12 Abs *vs.* conc. and % EC_{50} *vs.* conc. of BSA with EC_{50} of **AA**, **T1**, and **T2**.

sensitive site to react with the H^+ of the 2-methylphenol. So, **T0** was prepared in the THF and *t*-BuOK medium by releasing HCl. The THF and *t*-BuOK chemical species of the medium could not influence the structure of the TMC, except for allowing the participation of its Cl^- in the reaction. Similarly, the chemical species present in the medium used to synthesize **T0**, **T1**, and **T2** did not disrupt the TMC structure, except for allowing its Cl anion to participate in the reaction. Hence the TMC acted as a highly safe core as no part of it was involved in the reaction except for the Cl^-. Also, in the case of the **Ta** and **Tb** intermediates, these were allowed to react with the Cl through the –OH group of the TMC in the THF/*t*-BuOK medium (Schemes 11b and 12a), then no chemical species reacted with the other constituents of the TMC in the reaction to develop the **Ta** and **Tb** (Schemes 11b and 12a). The deprotection of **Ta** and **Tb** was conducted because the TMC was holding them as MTBDMSH (Scheme 10) and DTBDMSP (Scheme 12a and b). The Cl^- of the TMC developed a covalent bond with the O atom of the –OH groups of the MTBDMSH (Scheme 12a and b) and the DTBDMSP (Scheme 12a and b) through the ether hydrolysis. Thus, TMC is a safer and green core to successfully allow the reaction of the –OH groups with the Cl^- of the TMC and supported the deprotection through the hydrolysis processes without undergoing any structural transition, damage or destruction. It maintained its whole structure as such to support the required chemical processes. The TMC core also supported a slow and stepwise release of H^+ from the **T1** and **T2** dendrimers for scavenging the free radicals.

3.2.3. Use of dihydroxybenzenes alone as antioxidants. Dihydroxybenzenes have phenolic –OH groups which release protons (H^+) that accept an additional electron of free radicals. Logically it is correct that the dihydroxybenzenes catechol (1,2-dihydroxybenzene), resorcinol (1,3-dihydroxybenzene), and hydroquinone (1,4-dihydroxybenzenes) should be used to scavenge the free radicals in place of the **T1** and **T2** dendrimers. These dihydroxybenzenes release the H^+ ion in aqueous solutions and develop the phenolate anion ($C_6H_5O^-$) which is highly nucleophilic in nature. It strongly develops interactions as well as reactions with other chemical species used in the processes because the phenolate anion is of small size and its delocalization is also effective. Therefore, the phenolate anion spontaneously may develop several undesired chemical activities in the reaction mixture; for example, it could chelate the transitional metal cations Fe^{2+} and Fe^{3+} and others. These activities of the dihydroxybenzenes are inhibited when these are bonded with the TMC core through a covalent bond. Then the size is increased on using dihydroxybenzenes with TMC as the core with **T0**, **T1**, and **T2** dendrimers so undesired activities of the dihydroxybenzenes are not possible as the small sized dihydroxybenzene molecules are now not free. Their delocalization is also not so active because now it is used to support the TMC core linkages. These chemical linkages of the phenolic compounds with the TMC core have stabilized the slow release of the H from the **T1** and **T2** dendrimers. The **T1** and **T2** are of larger sizes and no effect of the phenolate ion in the case of the TMC core remained operational. The extended delocalization of the **T1** and **T2** have been buffering the activities over the use of the dihydroxybenzenes alone for scavenging free radicals. The delocalization remains the prominent factor and it could induce electron–electron repulsion with the phenolate ion as it has a negatively charged center at the benzene ring and, also has a negative charge on the O atom outside the ring on releasing H^+. Therefore, the use of dihydroxybenzenes alone is not advisable for antioxidant activities as the chemical processes of the scavenging are sensitive towards the presence of chemical species which are not of any use.

3.3 BSA and lysozyme

Dendrimers interact with proteins and lyso through their peptide bonds or electrostatic forces with synergetic effects on the EC_{50} of the dendrimers with variable concentration. 1, 3, and 5 mg mL^{-1} stock solutions of BSA and lyso were prepared with water and 100, 200, 300, 400, and 500 μl volumes were made up to 0.5 ml portions of both the BSA and lyso stock solutions, separately. These were added to DPPH solution separately containing the EC_{50} of **AA**, **T1**, and **T2**, which did not aggregate BSA and lyso due to their critically low concentrations.[34,35] BSA was from 0.606 to 0.152 μM and the lyso was from 2.8 to 0.70 μM. With **AA**, on increasing the BSA concentration, the EC_{50} value is increased by 41.50% and later decreased to

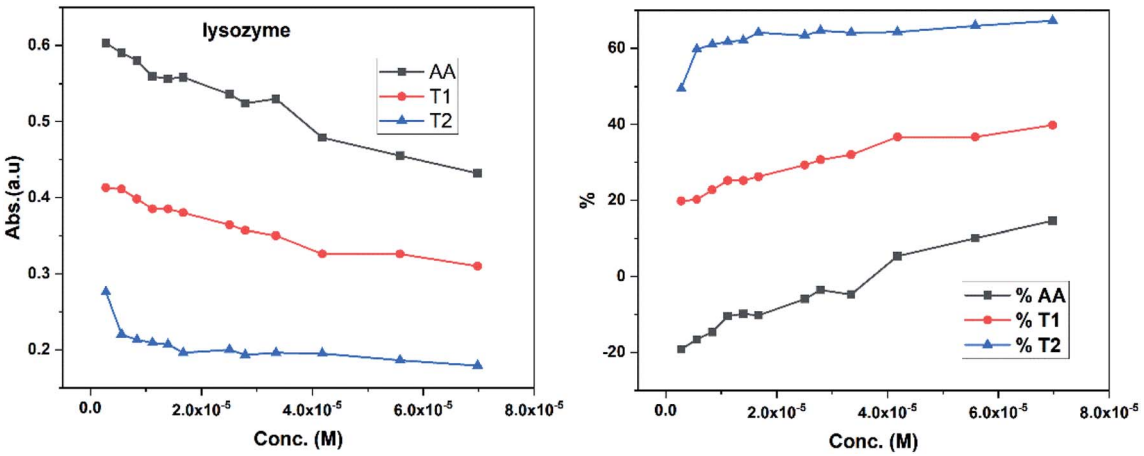

Fig. 13 Abs *vs.* conc. and % EC *vs.* conc. graph of lyso with EC_{50} AA, T1, and T2.

25.30%. With **T1**, the EC_{50} is increased to 39.03% and decreased to −34.37%. With **T2**, the EC_{50} decreased by −39.74% and then increased to 155.86%. Fig. 12 and 13 show that **AA** and **T1** both initially induce a dispersive effect, but on increasing the BSA concentration the dispersion is weakened. However, with **T2**, initially it synergized but later it is weakened due to opposing reorientations. After 3.03 μM BSA with **T2**, it was precipitated due to aggregation of the BSA within the void spaces of **T2** as the solvent could not bind so the BSA opted to aggregate within the voids of **T2**. The proteins with lower additive concentrations 'salt in' but those with higher concentration 'salt out' due to aggregation. This did not occur with **AA** and **T1** on adding BSA, which predicts a role of the two –OH of **T2** in aggregating the BSA. Also the BSA has reduced scavenging limits contrary to **AA**. Thus, the BSA has entered the robust hydrophobic void spaces of both **T1** and **T2** (Fig. 5). **T1** and **T2** have both aggregated BSA and lyso, which has hampered their scavenging activities (Fig. 12). **AA** is quickly protonated forming H_3O^+ (hydronium) ions with water molecules, which catalyzed scavenging with BSA and lyso aqueous solutions (Fig. 13 and 14).

Abs for increasing BSA concentrations saturates at ~6 μM in response to UV/Vis light and is diminished because BSA might have aggregated within the voids spaces of **T2**. Fig. 12 gives abs = 0.3 for blank and abs for ~6 μM BSA = 1.3 with **T2**; putting these values in eqn (8), **T2** aggregated 79.92% of BSA, contrary to 43.5% with **T1**. The BSA aggregating activities fractionate the scavenging activities of **T1** and **T2**. Unlike BSA, the lyso with **AA**, **T1**, and **T2** got aggregated in **T2** > **T1** > **AA** order. **T2** aggregated ~60% lyso compared to 79.92% BSA. Stronger binding of BSA and lyso with **T2** than **T1** occurred due its 2-OH.

The water which bound BSA and lyso in their aqueous solutions without mixing with **AA** is now available for **AA** molecules. Even mildly protic methanol molecules were in close chemical contact with **AA**, which is now engaged by a proton in the resultant sample. The **AA** got free and interacts with BSA, while on the other hand the **T1** and **T2** both aggregate BSA and lyso in the void spaces. Now the **T1** and **T2** are engaged with BSA and lyso in holding them in the void spaces, rather than releasing H^+ that scavenges the DPPH radicals. Fig. 12 depicts abs with increasing BSA concentration with the EC_{50} of **AA**, **T1**, and **T2**. Abs with **T2** for lower concentrations exponentially increases due to BSA dispersion but when its concentration continuously increases, then the BSA molecules tend to occupy the void spaces, which activates the electronic transitions. This could interrupt extended conjugations due to 2-OH with **T2**. Also the BSA molecules may partially move towards the void

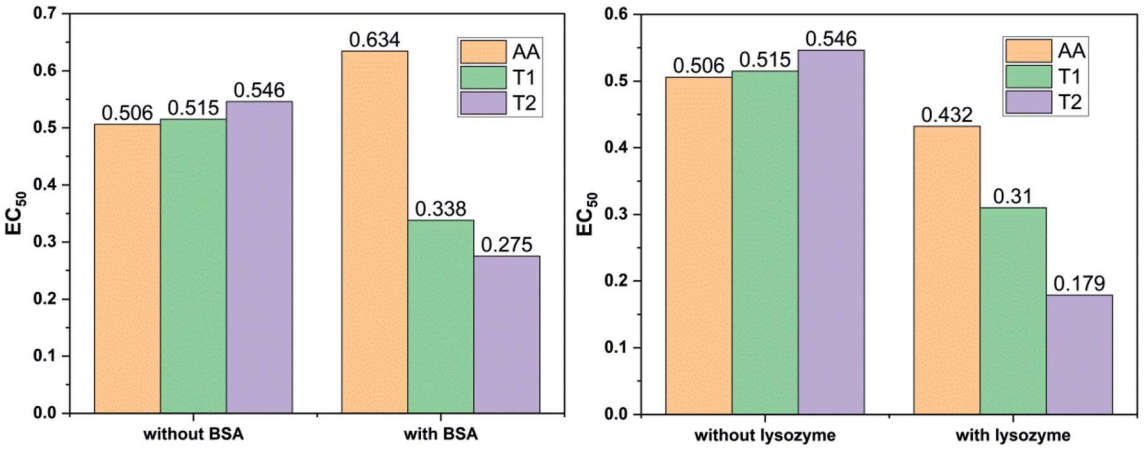

Fig. 14 BSA and lysozyme inhibit free radical scavenging in aqueous menthol solutions.

spaces and later get aggregated with variable orientational vibrations which absorb UV/Vis light (Fig. 13). The **AA** and **T1** did not absorb much UV/Vis light on increasing the BSA concentration as these do not have complicated pi-conjugations. In particular, the **T1** has only 1-OH so the extended conjugations are not interrupted and a single electronic chain from HOMO to LUMO occurred contrary to 2-OH of **T2**. Also the 2HOMO to 2LUMO for each –OH might be materialized simultaneously, which absorbs more UV/Vis light (Fig. 14). Abs is **T2** > **AA** > **T1**; the **AA** has no pi-conjugation but releases two H^+ which absorb more UV/Vis light than even the simple extended conjugation of **T1**, while **T2** has 2-OH and absorbed more UV/Vis light.

Increasing concentrations of lyso with EC_{50} of **AA**, **T1** and **T2** have absorb UV/Vis light in the order of **AA** > **T1** > **T2**. The lyso has less amino acids in its structure and strongly interacted with **AA** and absorbed more UV/Vis light, but **T2** might have aggregated lyso within its void spaces. So it may not allow excitation as a stronger aggregation developed stronger potential energy, which defuncts and opposes electronic transitions. Lyso aggregation is as **T2** > **T1** > **AA**; **T1** induced a synergetic effect with BSA, while **AA** produced a less synergetic effect, but **T2** has an opposing effect with BSA. With lyso, the EC_{50} value of **AA** increased to 19.17% with increasing lyso concentration and later it decreased to −14.62%. The EC_{50} value with **T1** is decreased to −19.80% and also decreased to −39.81% and with **T2**, the EC_{50} decreased to −49.45% and then decreased to −67.21%. Lyso is a competitive component to decrease the EC_{50} value of the dendrimers.

4. Conclusion

T0, **T1** and **T2** dendrimers as potential antioxidants have scavenged DPPH radicals studied spectrophotometrically. The scavenging abilities of **T2** with 6-OH are 10 times higher than that of **T1** with 3-OH. The **AA** showed a higher antioxidant activity than **T1** and **T2** due to its faster electronic reorientation to quickly release H^+ with a higher resonance. Dendrimers acted as smart hydrophobes with hydrophobically functional void spaces. To reduce chemical waste and increase yield, branching units were synthesized *via* selective protection and deprotection routes. BSA and lysozyme both showed good interaction with the dendrimers compared to standard **AA**. Lyso acted as a promising protein to give a synergetic effect. These proteins increased the antioxidant activities of the dendrimers. The results significantly reveal a mechanism for effective biodegradable dendrimers, bioremediation, drug efficacy, and protein interacting capacity. **T0**, **T1** and **T2** dendrimers with 0, 3 and 6-OH groups have potential to further engage –OH groups to initiation condensation reactions in a suitable medium to develop macromolecules.

Conflicts of interest

There are no conflicts to declare.

Acknowledgements

The authors are thankful to the Central University of Gujarat for infrastructures. Dhaval Makawana acknowledges RGNF awarded (F1-17.1/2015-16/RGNF-2015-17-SC-GUJ-24172/(SA-III/Website)) for financial support.

References

1 R. K. Ameta and M. Singh, A thermodynamic in vitro antioxidant study of vitamins B (niacin and niacin amide) and C (ascorbic acid) with DPPH through UV spectrophotometric and physicochemical methods, *J. Mol. Liq.*, 2014, **195**, 40–46, DOI: 10.1016/j.molliq.2014.01.029.

2 N. C. Cook and S. Samman, Flavonoids—chemistry, metabolism, cardioprotective effects, and dietary sources, *J. Nutr. Biochem.*, 1996, **7**, 66–76, DOI: 10.1016/S0955-2863(95)00168-9.

3 O. I. Aruoma, Characterization of drugs as antioxidant prophylactics, *Free Radic. Biol. Med.*, 1996, **20**, 675–705, DOI: 10.1016/0891-5849(95)02110-8.

4 N. Vashistha, A. Chandra and M. Singh, Influence of rhodamine B on interaction behaviour of lanthanide nitrates with 1st tier dendrimer in aqueous DMSO: a physicochemical, critical aggregation concentration and antioxidant activity study, *J. Mol. Liq.*, 2018, **260**, 323–341, DOI: 10.1016/j.molliq.2018.03.056.

5 F. Shahidi and Y. Zhong, Measurement of antioxidant activity with .pdf, *J. Funct. Foods*, 2015, **18**, 757–781, DOI: 10.1016/j.jff.2015.01.047.

6 B. N. Dar, S. Sharma and G. A. Nayik, Effect of storage period on physiochemical, total phenolic content and antioxidant properties of bran enriched snacks, *J. Food Meas. Charact.*, 2016, **10**, 755–761, DOI: 10.1007/s11694-016-9360-x.

7 B. Halliwell, Antioxidant characterization. Methodology and mechanism, *Biochem. Pharmacol.*, 1995, **49**, 1341–1348, DOI: 10.1016/0006-2952(95)00088-H.

8 H. M. Ali, A. Abo-Shady, H. A. Sharaf Eldeen, H. A. Soror, W. G. Shousha, O. A. Abdel-Barry and A. M. Saleh, Structural features, kinetics and SAR study of radical scavenging and antioxidant activities of phenolic and anilinic compounds, *Chem. Cent. J.*, 2013, **7**, 1–9, DOI: 10.1186/1752-153X-7-53.

9 P. Malik and M. Singh, Study of curcumin antioxidant activities in robust oil-water nanoemulsions, *New J. Chem.*, 2017, **41**, 12506–12519, DOI: 10.1039/c7nj02612a.

10 R. A. Gossage, E. Munoz-Martinez, H. Frey, A. Burgath, M. Lutz, A. L. Spek and G. Van Koten, A novel phenol for use in convergent and divergent dendrimer synthesis: access to core functionalizable trifurcate carbosilane dendrimers-the X-ray crystal structure of [1,3,5-tris{4-(triallylsilyl)phenyl ester}benzene], *Chem.–Eur. J.*, 1999, **5**, 2191–2197, DOI: 10.1002/(SICI)1521-3765(19990702)5:7<2191::AID-CHEM2191>3.0.CO;2-J.

11 K. Esumi, H. Houdatsu and T. Yoshimura, Antioxidant action by gold-PAMAM dendrimer nanocomposites, *Langmuir*, 2004, **20**, 2536–2538, DOI: 10.1021/la036299r.

12 C. Li, P. Sun, H. Yu, N. Zhang and J. Wang, Scavenging ability of dendritic PAMAM bridged hindered phenolic antioxidants towards DPPH˙ and ROO˙ free radicals, *RSC Adv.*, 2017, **7**, 1869–1876, DOI: 10.1039/c6ra26134e.

13 C. Y. Lee, A. Sharma, J. E. Cheong and J. L. Nelson, Synthesis and antioxidant properties of dendritic polyphenols, *Bioorg. Med. Chem. Lett.*, 2009, **19**, 6326–6330, DOI: 10.1016/j.bmcl.2009.09.088.

14 J. Handique and D. Mahanta, Synthesis and Electrochemical Behavior of Some Dendritic Polyphenols as Antioxidants, *Lett. Org.*, 2013, **2370210**, 53–59, http://www.ingentaconnect.com/content/ben/loc/2013/00000010/00000001/art00013.

15 K. Rajavelu, M. Subaraja and P. Rajakumar, Synthesis, optical properties, and antioxidant and anticancer activity of benzoheterazole dendrimers with triazole bridging unit, *New J. Chem.*, 2018, **42**, 3282–3292, DOI: 10.1039/c7nj04060a.

16 J. D. amou, K. Twibanire and T. B. Grindley, Polyester dendrimers, *Polymers*, 2012, **4**, 794–879, DOI: 10.3390/polym4010794.

17 D. Liu, J. Shi, A. Colina Ibarra, Y. Kakuda and S. Jun Xue, The scavenging capacity and synergistic effects of lycopene, vitamin E, vitamin C, and β-carotene mixtures on the DPPH free radical, *LWT - Food Sci. Technol.*, 2008, **41**, 1344–1349, DOI: 10.1016/j.lwt.2007.08.001.

18 A. J. Young and G. M. Lowe, Antioxidant and Prooxidant Properties of Carotenoids, *Arch. Biochem. Biophys.*, 2001, **385**, 20–27, DOI: 10.1006/abbi.2000.2149.

19 T. Nishiyama, T. Sugimoto and Y. Andoh, Antioxidant activity of phenols in intramolecularly cooperating stabilizing systems, *Polym. Degrad. Stab.*, 2001, **74**, 189–193, DOI: 10.1016/S0141-3910(01)00151-3.

20 T. Nishiyama, Y. Andoh, T. Sugimoto and T. Okamoto, New bifunctional antioxidants—intramolecular synergistic effects between chromanol and thiopropionate groups, *Polym. Degrad. Stab.*, 2003, **81**, 409–413, DOI: 10.1016/S0141-3910(03)00125-3.

21 P. Suresh, S. Srimurugan, B. Babu and H. N. Pati, Asymmetric sulfoxidation of prochiral sulfides using aminoalcohol derived chiral C_3-symmetric trinuclear vanadium Schiff base complexes, *Tetrahedron: Asymmetry*, 2007, **18**, 2820–2827.

22 V. Thavasi, L. P. Leong and R. P. A. Bettens, Investigation of the influence of hydroxy groups on the radical scavenging ability of polyphenols, *J. Phys. Chem. A*, 2006, **110**, 4918–4923, DOI: 10.1021/jp057315r.

23 E. N. Khimich, G. S. Buslaev, A. V Zdravkov, N. N. Khimich and M. G. Voronkov, Polysiloxane Structures Cross-Linked with Hydroquinone and Phloroglucinol, *Russ. J. Appl. Chem.*, 2008, **81**, 1070–4272, DOI: 10.1134/S107042720808017X.

24 W. Brand-Williams, M. E. Cuvelier and C. Berset, Use of a free radical method to evaluate antioxidant activity, *LWT - Food Sci. Technol.*, 1995, **28**, 25–30, DOI: 10.1016/S0023-6438(95)80008-5.

25 R. J. Elias, S. S. Kellerby and E. A. Decker, Antioxidant activity of proteins and peptides, *Crit. Rev. Food Sci. Nutr.*, 2008, **48**, 430–441, DOI: 10.1080/10408390701425615.

26 R. T. Dean, S. Fu, R. Stocker and M. J. Davies, Biochemistry and pathology of radical-mediated protein oxidation, *Biochem. J.*, 1997, **324**(1), 1–18, DOI: 10.1042/bj3240001.

27 M. P. Almajano and M. H. Gordon, Synergistic Effect of BSA on Antioxidant Activities in Model Food Emulsions, *J. Am. Oil Chem. Soc.*, 2004, **81**, 1–6, DOI: 10.1007/s11746-004-0895-6.

28 M. Yang, Y. Wu, J. Li, H. Zhou and X. Wang, Binding of curcumin with bovine serum albumin in the presence of ι-carrageenan and implications on the stability and antioxidant activity of curcumin, *J. Agric. Food Chem.*, 2013, **61**, 7150–7155, DOI: 10.1021/jf401827x.

29 M. Voicescu, G. Neacsu, A. Beteringhe, O. Craciunescu, R. Tatia and L. Moldovan, Antioxidant and cytotoxic properties of riboflavin in PEG/BSA systems, *Chem. Pap.*, 2017, **71**, 1107–1117, DOI: 10.1007/s11696-016-0057-8.

30 S. J. You, C. C. Udenigwe, R. E. Aluko and J. Wu, Multifunctional peptides from egg white lysozyme, *Food Res. Int.*, 2010, **43**, 848–855, DOI: 10.1016/j.foodres.2009.12.004.

31 H. Liu, Amelioration of oxidant stress by the defensin lysozyme, *Am. J. Physiol. Endocrinol. Metabol.*, 2006, **290**, E824–E832, DOI: 10.1152/ajpendo.00349.2005.

32 P. Sharma and R. P. Singh, Evaluation of antioxidant activity in foods with special reference to TEAC method, *Am. J. Food Technol.*, 2013, **8**, 83–101, DOI: 10.3923/ajft.2013.83.101.

33 A. K. Jangid, D. Pooja and H. Kulhari, Determination of solubility, stability and degradation kinetics of morin hydrate in physiological solutions, *RSC Adv.*, 2018, **8**, 28836–28842, DOI: 10.1039/c8ra04139c.

34 A. Lo, P. Wentworth, F. Sieber, W. A. Metz and K. D. Janda, Soluble Polymer-Supported Chemoenzymatic Synthesis of the C21–C7 Fragment of the Bryostatins, *J. Org. Chem.*, 2000, **65**, 8527–8531, DOI: 10.1021/jo005539u.

35 G. Houen, K. Bechgaard, K. Bechgaard, J. Songstad, M. Leskelä, M. Polamo, M. N. Homsi, F. K. H. Kuske, M. Haugg, N. Trabesinger-Rüf and E. G. Weinhold, The Solubility of Proteins in Organic Solvents, *Acta Chem. Scand.*, 1996, **50**, 68–70, DOI: 10.3891/acta.chem.scand.50-0068.

